

From Non-Identifiability to Goal-Integrated Decision-Making in Parametric Inverse Optimization

Farzin Ahmadi, Fardin Ganjkhanloo, Kimia Ghobadi

Department of Civil and Systems Engineering, The Center for Systems Science and Engineering, The Malone Center for Engineering in Healthcare, Johns Hopkins University, Baltimore, MD 21218, fahmadi1@jhu.edu, fganjkh1@jhu.edu, kimia@jhu.edu

Inverse optimization seeks to recover unknown objective parameters from observed decisions, yet fundamental questions about when recovery is possible have received limited formal treatment. This paper develops a comprehensive theoretical framework for inverse optimization in parametric convex models. We first establish that non-identifiability is the generic case: even with normalization and multiple observations, the parameter set compatible with data is generically multi-dimensional, and regularization does not resolve this. We derive necessary and sufficient conditions for identifiability. Motivated by these negative results, we introduce the Inverse Learning (IL) framework, which shifts the inferential target from the unknown parameter to the latent optimal solution, achieving a complexity reduction that is independent of the number of observations. \mathcal{IL} explicitly characterizes the full set of compatible parameters rather than returning an arbitrary element. To address the tension between observational fidelity and constraint adherence, we formalize the Observation-Constraint Tradeoff and develop Goal-Integrated Inverse Learning models that enable structured navigation of this spectrum with guaranteed monotonicity. Numerical experiments demonstrate superior solution accuracy, higher parameter recovery rates, and significant computational speedups. We apply the framework to personalized dietary recommendations using NHANES data, proof-of-concept demonstrating improved glycemic control in a prospective feasibility study.

Key words: inverse optimization, parametric convex optimization, data-driven decision-making

¹F. Ahmadi is currently at the Department of Health Sciences, Towson University, Towson, MD 21252.

¹F. Ganjkhanloo is currently at the Center for Health Systems and Policy Modeling, Johns Hopkins University, Washington DC 20001.

1. Introduction

A fundamental question in operations research is how to infer the objectives driving observed decisions. When a decision-maker repeatedly solves an optimization problem whose constraints are known but whose objective function is not, the *inverse optimization* problem seeks to recover the unknown parameters from observed solutions. Since the seminal formulation by [Ahuja and Orlin \(2001\)](#), inverse optimization has grown into a mature methodological area with applications spanning healthcare ([Chan et al. 2014](#), [Ajayi et al. 2022](#)), transportation ([Chow and Recker 2012](#)), energy systems ([Saez-Gallego et al. 2017](#), [Ratliff et al. 2014](#)), and finance ([Bertsimas et al. 2012](#), [Utz et al. 2014](#)). Recent surveys ([Chan et al. 2024](#), [Heuberger 2004](#)) and methodological advances in statistical consistency ([Aswani et al. 2018](#)), online learning ([Dong et al. 2018](#), [Besbes et al. 2023](#)), loss function design, and uncertainty quantification ([Lin and Others 2024](#)) have substantially expanded the field's scope and rigor.

Despite this progress, two challenges have impeded the practical deployment of inverse optimization in data-rich settings. The first is *non-identifiability*: when can the unknown objective parameters be uniquely recovered from observed decisions, and what happens when they cannot? The issue has been acknowledged in specific contexts, for instance, [Aswani et al. \(2018\)](#) noted that constraints can render parameters unidentifiable, and [Chan et al. \(2019\)](#) developed closed-form solutions under special structures. However, a systematic characterization of when and why identifiability fails in general convex models has been lacking. The second challenge is *computational scalability*: classical KKT-based inverse formulations have variables and constraints scaling linearly with the number of observations. For modern applications with thousands of observations, this scaling renders standard formulations impractical.

This paper addresses both challenges within a unified framework for parametric convex optimization. We adopt a structured objective with known convex basis functions and an unknown parameter vector, encompassing linear programs, convex quadratic programs, and broader convex models as special cases. Our contributions are organized around three interconnected themes.

1.1. Contributions

1. Non-identifiability is the generic case. We provide, to our knowledge, the first comprehensive non-identifiability analysis for inverse optimization in parametric convex models. For linear programs, we characterize identifiability through the geometry of normal cone intersections: parameter uniqueness requires the common normal cone to collapse to a single ray ([Theorem 1](#)), a condition that is generically violated whenever observations share two or more non-collinear active constraint normals ([Proposition 2](#)). For general convex models, we identify two distinct sources of

ambiguity, namely, normal cone dimensionality and basis function degeneracy, and show that the parameter feasibility set \mathcal{S} is a polyhedral cone whose dimension depends on both the gradient structure and the constraint geometry (Theorem 2). Critically, regularization does not resolve non-identifiability; it can only enlarge the feasible parameter set (Corollary 1). We then establish sharp sufficient conditions for identifiability based on a novel *orthogonal persistent excitation* condition: the excitation matrix must be positive definite (Theorem 3). This condition is both necessary and sufficient (Proposition 5), precisely separating the identifiable and non-identifiable components of the data's information content.

2. Inverse Learning: scalability and solution identifiability. Motivated by the prevalence of non-identifiability and the computational burden of classical formulations, we introduce *Inverse Learning* (IL). Rather than imputing separate optimal solutions for each observation (as in classical inverse optimization), \mathcal{IL} learns a *single representative optimal solution* that minimizes aggregate distance to observations while satisfying the KKT conditions for some parameter. This reformulation achieves two key properties. First, problem complexity drops to linear order of variables and constraints of the forward problem, *independent of the number of observations K* (Theorem 4). For squared Euclidean loss, the data enter only through the sample centroid (Proposition 6), enabling streaming updates, parallelization, and memory-efficient implementations. Second, \mathcal{IL} achieves *solution identifiability* (uniqueness of the recovered optimal solution) -under conditions that are strictly different from, and in many practical settings less restrictive than, those required for parameter identifiability (Theorem 7). \mathcal{IL} does not require one-dimensional normal cones or excitation conditions; it requires only local convexity of the optimality set near the true solution. Rather than returning an arbitrary feasible parameter, \mathcal{IL} explicitly characterizes the full set of compatible parameters (Theorem 5), making non-uniqueness transparent.

3. The Observation-Constraint Tradeoff and Goal-Integrated models. We formalize the tension between fitting observed behavior and enforcing domain constraints as the *Observation-Constraint Tradeoff* (Definition 2) and develop *Goal-Integrated Inverse Learning* models to navigate it. \mathcal{GIL} controls the number r of binding relevant constraints via a cardinality parameter, enabling systematic exploration of the tradeoff spectrum. \mathcal{MGIL} provides structured sequential navigation by iteratively adding constraints while inheriting previously active ones, yielding monotone distance sequences (Theorem 10) over nested faces (Theorem 11). Both models preserve the K -independence of \mathcal{IL} , enforce complete KKT conditions guaranteeing forward optimality, and characterize the compatible parameter set at each solution. A constraint hierarchy—relevant (expert knowledge), preferred (priority subset), and trivial (structural feasibility)—supports data-driven constraint selection while maintaining mathematical validity.

1.2. Relevant Literature

The inverse optimization literature has evolved along several interrelated threads. The classical strand, initiated by [Ahuja and Orlin \(2001\)](#) and developed by [Heuberger \(2004\)](#), [Iyengar and Kang \(2005\)](#), [Chan et al. \(2014\)](#), focuses on recovering parameters under the assumption that observations are exactly optimal. The data-driven strand relaxes this assumption, accommodating noisy or suboptimal observations through loss-function-based formulations ([Keshavarz et al. 2011](#), [Bertsimas et al. 2015](#), [Aswani et al. 2018](#), [Esfahani et al. 2018](#)). Recent work has further extended these foundations: [Besbes et al. \(2023\)](#) develop offline and online contextual inverse optimization with logarithmic regret bounds, introducing the circumcenter policy and ellipsoidal cone machinery for minimax regret; [Zattoni Scroccaro et al. \(2025\)](#) propose the complementary incenter cost vector with tractable convex reformulations, introduce the augmented suboptimality loss (ASL) as a relaxation for inconsistent data, and develop a stochastic approximate mirror descent algorithm with provable convergence rates; [Lin and Others \(2024\)](#) propose conformal inverse optimization, learning uncertainty sets rather than point estimates; and [Shahmoradi and Lee \(2022\)](#) develop quantile-based approaches to improve stability.

Our work intersects with but is distinct from these contributions in several respects. First, while identifiability has been discussed as a technical assumption supporting consistency results ([Aswani et al. 2018](#)) or as a geometric property of specific models ([Chan et al. 2019](#)), we provide a systematic analysis establishing that non-identifiability is structurally inherent in inverse convex optimization. Our orthogonal excitation condition offers a precise geometric characterization that unifies and extends scattered conditions in the literature. Second, whereas classical and data-driven approaches both scale linearly in K , our \mathcal{IL} framework eliminates this dependence entirely through a reformulation that targets the latent solution rather than the parameter—a fundamentally different inferential objective. Third, the Goal-Integrated framework addresses a gap largely unaddressed in the inverse optimization literature: the integration of domain expertise through constraint hierarchies and controlled constraint activation, providing practitioners with interpretable mechanisms to balance data fidelity against normative goals.

The observation-constraint tradeoff that we formalize also connects to the broader literature on decision-aware learning ([Elmachtoub and Grigas 2022](#)) and prescriptive analytics, where the goal is not merely to estimate parameters but to generate actionable decisions. Our framework provides a structured path from descriptive (what do people do?) through normative (what should they do?) to prescriptive (what achievable changes would improve outcomes?), a progression of particular value in behavioral applications.

From an application perspective, personalized health interventions and dietary recommendations in particular represent a natural domain for inverse optimization. Observed dietary behaviors reflect

latent preferences that may conflict with clinical guidelines, and the gap between population-level recommendations and individual adherence remains a significant challenge (Sacks et al. 2001, Liese et al. 2009). Our framework addresses this gap by generating recommendations that respect habitual patterns while progressively incorporating nutritional constraints, with each step quantifying the marginal behavioral cost of additional guideline adherence.

The remainder of this paper is organized as follows. Section 2 formalizes the inverse optimization problem for parametric convex models, establishes the non-identifiability results, and derives identifiability conditions. Section 3 develops the Inverse Learning framework, including complexity reduction, statistical guarantees, and solution identifiability. Section 4 introduces the Goal-Integrated models (GIL and \mathcal{MGIL}) and the Observation-Constraint Tradeoff. Section 5 presents numerical experiments comparing the \mathcal{IL} framework against classical inverse optimization. Section 6 applies the methodology to personalized dietary recommendations using NHANES data and a prospective feasibility study. Section EC.2 in the electronic companion describes the interactive decision-support tools developed to operationalize the framework.

2. Inverse Optimization for Parametric Convex Models

2.1. Preliminaries

We adopt a structured parametric objective of the form

$$f(x, \theta) = \sum_{j=1}^p \theta_j \phi_j(x), \quad (1)$$

where $\theta = (\theta_1, \dots, \theta_p)^\top \in \mathbb{R}^p$ are unknown parameters and $\phi_j : \mathbb{R}^n \rightarrow \mathbb{R}$ are known, continuously differentiable convex basis functions. To ensure that $\mathcal{FO}(\theta, \Omega)$ is a convex optimization problem for every admissible parameter vector, we restrict attention to nonnegative combinations of convex basis functions, i.e., $\theta \in \mathbb{R}_+^p$ (see Assumption 3). Under this restriction, $f(\cdot, \theta)$ is convex on Ω .

This parametric form covers several standard models: (i) for linear programs, $\phi_j(x) = x_j$ yields $f(x, \theta) = \theta^\top x$; and (ii) for convex quadratic programs, $\phi_j(x) = x^\top Q_j x$ with $Q_j \succeq 0$ (and optionally affine terms $\phi_j(x) = x_i$) yields $f(x, \theta) = x^\top (\sum_j \theta_j Q_j) x + c(\theta)^\top x$ with a positive semidefinite quadratic term. We base our methodology on the following assumptions.

ASSUMPTION 1 (Basis Function Properties). *We assume: (i) $\{\phi_j\}_{j=1}^p$ are linearly independent on Ω ; (ii) some ϕ_{j_0} is non-constant on Ω ; (iii) each ϕ_j is convex and continuously differentiable on Ω ; and (iv) the gradient matrix $[\nabla \phi_1(x) \ \cdots \ \nabla \phi_p(x)]$ has rank at least $\min(p, n)$ for generic $x \in \Omega$.*

ASSUMPTION 2 (Constraint Qualification and Smoothness). *The constraint functions $g_i : \mathbb{R}^n \rightarrow \mathbb{R}$ are convex and continuously differentiable. The feasible set $\Omega = \{x \in \mathbb{R}^n : g_i(x) \leq 0, i = 1, \dots, m\}$ satisfies Slater's condition: there exists $\hat{x} \in \mathbb{R}^n$ such that $g_i(\hat{x}) < 0$ for all i .*

ASSUMPTION 3 (**Parameter Normalization**). *To avoid scale invariance and preserve convexity of $f(\cdot, \theta)$, we restrict parameters to*

$$\Theta = \{\theta \in \mathbb{R}_+^p : \|\theta\|_q = 1, \theta_{j_0} \geq \alpha > 0\}, \quad (2)$$

where $q \in [1, \infty]$ and $\alpha > 0$ ensures the non-constant basis function ϕ_{j_0} receives nonzero weight.

Given noisy observations $\mathcal{X} = \{x^k : k = 1, \dots, K\}$, the inverse convex optimization problem seeks parameters θ such that each observation is close to an optimal solution of $\mathcal{FO}(\theta, \Omega)$. Under Assumption 2, the following KKT-based formulation enforces optimality:

$$\begin{aligned} \mathcal{ICO}(\mathcal{X}, \Omega) : \quad & \min_{\theta, \{\lambda^k\}, \{z^k\}} \sum_{k=1}^K \|x^k - z^k\|_2^2 \\ & \text{s.t. } z^k \in \Omega, \quad \forall k, \\ & \sum_{j=1}^p \theta_j \nabla \phi_j(z^k) + \sum_{i=1}^m \lambda_i^k \nabla g_i(z^k) = 0, \quad \forall k, \\ & \lambda_i^k g_i(z^k) = 0, \quad \forall i, k, \\ & \lambda^k \in \mathbb{R}_+^m, \quad \forall k, \quad \theta \in \Theta. \end{aligned} \quad (3)$$

This enforces the Karush–Kuhn–Tucker (KKT) conditions of the forward problem. As is well known from the literature on inverse linear and convex optimization (see, e.g., [Ahuja and Orlin 2001](#), [Chan et al. 2014](#), [Aswani et al. 2018](#)), this problem is generally nonconvex and NP-hard due to complementarity constraints. Under Slater’s condition (Assumption 2), the KKT conditions are both necessary and sufficient for optimality of z^k in the forward problem, and strong duality holds. When $\phi_j(x) = x_j$ and $g_i(x) = b_i - a_i^\top x$, the problem reduces to the classical inverse linear optimization model:

$$\begin{aligned} \mathcal{ICO}(\mathcal{X}, \Omega) : \quad & \min_{\theta, \{\lambda^k\}, \{z^k\}} \sum_{k=1}^K \|x^k - z^k\|_2^2 \\ & \text{s.t. } Az^k \geq b, \quad \forall k, \\ & \theta = A^\top \lambda^k, \quad \forall k, \\ & \theta^\top z^k = b^\top \lambda^k, \quad \forall k, \\ & \lambda^k \in \mathbb{R}_+^m, \quad \forall k, \quad \|\theta\|_q = 1. \end{aligned} \quad (4)$$

Note that in the linear case, the stationarity condition $\theta = A^\top \lambda^k$ combined with primal feasibility $Az^k \geq b$, dual feasibility $\lambda^k \geq 0$, and the strong duality equality $\theta^\top z^k = b^\top \lambda^k$ together imply complementary slackness: $\lambda_i^k (a_i^\top z^k - b_i) = 0$ for all i, k .

This formulation has been studied extensively (e.g., [Chan et al. 2014](#), [Bertsimas et al. 2015](#)) and admits tractable convex reformulations under certain norms and error measures. However,

computational scaling issues persist with large datasets. Following [Keshavarz et al. \(2011\)](#) and [Aswani et al. \(2018\)](#), a regularized version relaxes the KKT conditions by a tolerance $\epsilon > 0$:

$$\begin{aligned} \mathcal{R}\text{-ICCO}(\mathcal{X}, \Omega, \epsilon) : \quad & \min_{\theta, \{\lambda^k\}, \{z^k\}} \sum_{k=1}^K \|x^k - z^k\|_2^2 \\ & \text{s.t. } g_i(z^k) \leq \epsilon, \quad \forall i, k, \quad \lambda^k \in \mathbb{R}_+^m, \quad \forall k, \\ & \left\| \sum_{j=1}^p \theta_j \nabla \phi_j(z^k) + \sum_{i=1}^m \lambda_i^k \nabla g_i(z^k) \right\|_2 \leq \epsilon, \quad \forall k, \\ & \theta \in \Theta. \end{aligned} \tag{5}$$

This relaxation improves robustness to noise and avoids exact complementarity constraints. Under Assumptions 1–3, identifiability of θ requires sufficiently rich observations. If the basis evaluations $\{\phi_j(x^k)\}$ are linearly independent across k , then distinct parameters yield distinct objective functions, ensuring uniqueness up to normalization. Similar rank conditions appear in [Bertsimas et al. \(2015\)](#) and [Aswani et al. \(2018\)](#).

REMARK 1 (STATISTICAL CONSISTENCY). When observations are generated as $x^k = x^*(\theta_0) + \xi^k$ with zero-mean noise, estimators based on $\mathcal{R}\text{-ICCO}$ are statistically consistent under regularity conditions ([Aswani et al. 2018](#)). The convergence rate depends on the noise variance, the number of samples K , and the geometry of the basis functions. Consistency of the *parameter estimator* strictly requires the model to be identifiable. As we establish in Section 2.2, these identifiability conditions are generically violated in practice.

REMARK 2 (COMPUTATIONAL COMPLEXITY). For general convex basis functions, both ICCO and $\mathcal{R}\text{-ICCO}$ are nonconvex due to bilinearities in (3) and complementarity constraints; only local or heuristic methods are tractable in general. For the linear case with affine ϕ_j and g_i , the relaxed formulation $\mathcal{R}\text{-ICCO}$ reduces to a convex quadratic or second-order cone program, hence polynomial-time solvable via interior-point methods. The exact formulation ICCO remains NP-hard even in the linear case due to complementarity constraints. For quadratic or nonlinear forward models, $\mathcal{R}\text{-ICCO}$ remains biconvex, and global tractability is not guaranteed; in practice, alternating optimization and convex relaxations are used ([Aswani et al. 2018](#)).

When $\mathcal{FO}(\theta, \Omega)$ admits multiple optimal solutions, the inverse formulation imputes variables z^k that project each observation x^k onto the corresponding optimal set, thereby resolving nonuniqueness of solutions for a fixed θ . However, even with multiple (possibly noisy) observations, more than one parameter vector θ often rationalizes the data equally well. In linear models, any objective vector within the cone spanned by active constraint normals yields the same optimal face. The inverse optimization framework mitigates this ambiguity by enforcing joint consistency

across all samples and by imposing normalization, but uniqueness of θ is rarely guaranteed. As such, the feasible set of parameters may remain large, and the solution to \mathcal{ICO} or $\mathcal{R-ICO}$ should be interpreted as one element of a potentially non-unique set.

2.2. Non-Identifiability of \mathcal{ICO} and $\mathcal{R-ICO}$

In general, the inverse problems \mathcal{ICO} and $\mathcal{R-ICO}$ are *set-valued*, i.e., even with normalization, the parameter $\theta \in \Theta$ compatible with a dataset need not be unique. We establish this for the inverse linear case and then extend the analysis to general convex models. Let $\Omega = \{x \in \mathbb{R}^n : Ax \geq b\}$ with rows a_i^\top of $A \in \mathbb{R}^{m \times n}$, and let $f(x, \theta) = \theta^\top x$ (i.e., $\phi_j(x) = x_j$). For $z \in \Omega$, let $I(z) := \{i : a_i^\top z = b_i\}$ denote the active set, and let $N_\Omega(z) = \text{cone}\{a_i : i \in I(z)\}$ be the normal cone at z . The forward KKT conditions imply that any optimal z must satisfy $\theta \in N_\Omega(z)$, up to scaling.

PROPOSITION 1 (Normal Cone Intersection Structure). *Let $\{z^k\}_{k=1}^K \subseteq \Omega$ be imputed optima. Define the common normal cone intersection*

$$\mathcal{C} := \bigcap_{k=1}^K N_\Omega(z^k).$$

Then \mathcal{C} is a polyhedral cone. Moreover, let $I_\cap := \bigcap_{k=1}^K I(z^k)$ denote the common active set. Then:

- (i) $\text{cone}\{a_i : i \in I_\cap\} \subseteq \mathcal{C}$.
- (ii) If $I_\cap \neq \emptyset$, then \mathcal{C} is nonempty.
- (iii) \mathcal{C} reduces to a single ray if and only if $\dim(\mathcal{C}) = 1$.

The following proposition establishes explicit conditions under which \mathcal{C} contains multiple rays, which is the key requirement for non-identifiability.

PROPOSITION 2 (Conditions for Multiple Rays in \mathcal{C}). *Let $\mathcal{C} = \bigcap_{k=1}^K N_\Omega(z^k)$ and let $I_\cap = \bigcap_{k=1}^K I(z^k)$. The cone \mathcal{C} contains at least two distinct rays under any of the following conditions:*

- (i) (Rich common active set) $|I_\cap| \geq 2$ and the vectors $\{a_i : i \in I_\cap\}$ are not all collinear, i.e., $\dim(\text{span}\{a_i : i \in I_\cap\}) \geq 2$.
- (ii) (Single observation at non-simple vertex) $K = 1$ and $|I(z^1)| \geq 2$ with $\{a_i : i \in I(z^1)\}$ not all collinear.
- (iii) (Aligned active sets) For all k , the active sets satisfy $I(z^1) \subseteq I(z^k)$, and condition (ii) holds for z^1 .

Conversely, \mathcal{C} is a single ray if and only if $\dim(\mathcal{C}) = 1$, which requires the observations to collectively impose sufficient linearly independent restrictions on feasible objective directions to leave exactly one degree of freedom.

Condition (ii) of Proposition 2 is satisfied at any vertex of a polyhedron in \mathbb{R}^n where at least n constraints are active with linearly independent normals (the generic case). Even with multiple observations, condition (i) holds whenever all observations share at least two non-collinear active constraint normals—a common occurrence when observations cluster near a particular face or vertex. The single-ray case $\dim(\mathcal{C}) = 1$ is thus non-generic and requires precise geometric alignment across observations. We now state the main non-identifiability theorem for inverse linear programming.

THEOREM 1 (Non-Identifiability of \mathcal{ICO} in Linear Programs). *Let $\{z^k\}_{k=1}^K \subseteq \Omega$ be imputed optima and let $\mathcal{C} = \bigcap_{k=1}^K N_\Omega(z^k)$. If any of the conditions in Proposition 2 hold, then the feasible set $\mathcal{C} \cap \Theta$ contains at least two distinct points for any normalization set Θ of the form $\Theta = \{\theta : \|\theta\|_2 = 1\}$ or $\Theta = \{\theta : \mathbf{1}^\top \theta = 1, \theta \geq 0\}$. Consequently, \mathcal{ICO} admits multiple feasible parameters for the same dataset, and the inverse problem is non-identifiable.*

COROLLARY 1 (Persistence of Non-Identifiability Under Regularization). *Under the conditions of Theorem 1, the feasible set of $\mathcal{R-ICO}(\mathcal{X}, \Omega, \epsilon)$ also contains multiple feasible θ for all $\epsilon \geq 0$. That is, regularization does not resolve the non-identifiability present in \mathcal{ICO} .*

We now extend the non-identifiability analysis to parametric convex objectives of the form $f(x, \theta) = \sum_{j=1}^p \theta_j \phi_j(x)$. Let $A(z) := [\nabla \phi_1(z) \cdots \nabla \phi_p(z)] \in \mathbb{R}^{n \times p}$ denote the matrix of basis function gradients evaluated at z . The KKT stationarity condition for z to be optimal can be written as

$$A(z)\theta \in -N_\Omega(z). \quad (6)$$

For a collection of imputed optima $\{z^k\}_{k=1}^K$, define the parameter feasibility set

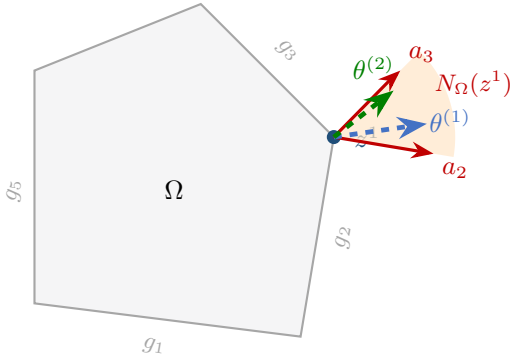
$$\mathcal{S} := \bigcap_{k=1}^K \{\theta \in \mathbb{R}^p : A(z^k)\theta \in -N_\Omega(z^k)\}. \quad (7)$$

PROPOSITION 3 (Feasibility Set Structure for Convex Models). *The set \mathcal{S} is a (possibly empty) polyhedral cone in \mathbb{R}^p . Its dimension depends on both the rank structure of the gradient matrices $\{A(z^k)\}_{k=1}^K$ and the dimensions of the normal cones $\{N_\Omega(z^k)\}_{k=1}^K$.*

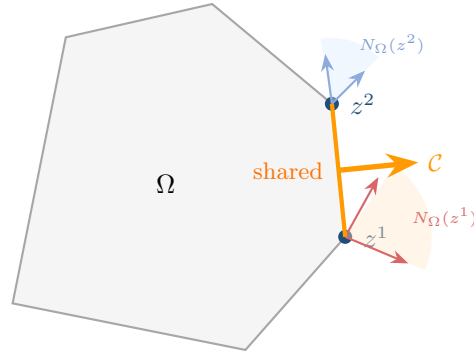
PROPOSITION 4 (Conditions for Non-Identifiability in Convex Models). *The set \mathcal{S} contains at least two non-collinear rays (hence $\mathcal{S} \cap \Theta$ contains multiple points for standard normalizations) under any of the following conditions:*

- (i) $\bigcap_{k=1}^K \ker(A(z^k)) \neq \{0\}$, i.e., there exists $\theta_0 \neq 0$ with $A(z^k)\theta_0 = 0$ for all k , and \mathcal{S} contains at least one element $\bar{\theta}$ not parallel to θ_0 .
- (ii) For some k_0 , $\dim(N_\Omega(z^{k_0})) \geq 2$, $A(z^{k_0})$ has full column rank p , and $\dim(\text{range}(A(z^{k_0})) \cap N_\Omega(z^{k_0})) \geq 2$

(a) Single observation at vertex



$|I(z^1)| = 2$ with non-collinear a_2, a_3
 $\Rightarrow \dim(N_\Omega(z^1)) = 2$
 \Rightarrow Multiple θ feasible (Prop. 2(ii))

(b) Intersection $\mathcal{C} = \bigcap_k N_\Omega(z^k)$ 

If $\dim(\mathcal{C}) = 1$: unique θ (up to scale)
 If $\dim(\mathcal{C}) \geq 2$: non-identifiable (Thm. 1)
 Generic case: $\dim(\mathcal{C}) \geq 2$

Figure 1 Geometric Illustration of non-identifiability in inverse linear optimization. (a) At a vertex z^1 where two non-collinear constraints are active, the normal cone $N_\Omega(z^1)$ is two-dimensional, admitting multiple feasible parameters $\theta^{(1)}, \theta^{(2)} \in N_\Omega(z^1) \cap \Theta$ (Proposition 2(ii)). (b) With two observations z^1, z^2 , the feasible parameter set is the intersection $\mathcal{C} = N_\Omega(z^1) \cap N_\Omega(z^2)$. Non-identifiability persists unless observations reduce \mathcal{C} to a single ray (Theorem 1).

(iii) The excitation matrix $S = \sum_{k=1}^K A(z^k)^\top P_k A(z^k)$ is singular, \mathcal{S} is non-empty, and there exists $\bar{\theta} \in \mathcal{S}$ not parallel to any $\Delta\theta \in \ker(S) \setminus \{0\}$.

The rank of the excitation matrix satisfies $\text{rank}(S) \leq \sum_{k=1}^K \text{rank}(P_k A(z^k)) \leq K(p-1)$ (each summand has rank at most $\min(n-1, p) \leq p-1$ under Assumption 5). Hence S is necessarily singular when $K(p-1) < p$, i.e., $K < p/(p-1)$. For $p \geq 2$ this gives $K < 2$, confirming the intuition that a single observation is generically insufficient for identifiability in multi-parameter models. More generally, for $S \succ 0$ one typically needs $K \geq p$ observations with sufficient geometric diversity (Corollary 2). The condition $\dim(\text{range}(A(z^{k_0})) \cap N_\Omega(z^{k_0})) \geq 2$ is automatically satisfied in the following cases: (a) Linear programs: $A(z) = I_n$ for all z , so $\text{range}(A) = \mathbb{R}^n$ and the condition reduces to $\dim(N_\Omega(z^{k_0})) \geq 2$. (b) Overparameterized models ($p \geq n$): $A(z^{k_0})$ maps \mathbb{R}^p onto \mathbb{R}^n , so again $\text{range}(A) = \mathbb{R}^n$. (c) Generic position with $p + \dim(N_\Omega(z^{k_0})) > n + 1$: a p -dimensional subspace generically intersects a d -dimensional cone in dimension $\max(p + d - n, 0)$, which is ≥ 2 when $p + d \geq n + 2$.

THEOREM 2 (Global Non-Identifiability in Convex Inverse Optimization). *If any of the conditions in Proposition 4 hold, then both ICO and R-ICO admit multiple feasible parameters θ , and the inverse problem is globally non-identifiable.*

REMARK 3 (SOURCES OF AMBIGUITY IN CONVEX MODELS). Equation (6) reveals two distinct sources of parameter ambiguity: (i) Normal cone dimensionality: If $N_\Omega(z^k)$ is high-dimensional (e.g., when z^k lies at a vertex with many active constraints), multiple objective gradient directions $-A(z^k)\theta$ can support the same optimum. (ii) Basis function degeneracy: If $A(z^k)$ is rank-deficient, then distinct parameter vectors θ can map to the same gradient $\nabla_x f(z^k, \theta)$. Uniqueness of θ requires both that the data sufficiently excite the basis directions (making the stacked matrix $[A(z^1)^\top \cdots A(z^K)^\top]^\top$ have full column rank) *and* that the intersection of normal cones collapse to a single ray. Absent these strong conditions—which are generically violated—the inverse problem remains set-valued.

In $\mathcal{R}\text{-ICO}$, the exact stationarity condition (6) is relaxed to $\text{dist}(A(z^k)\theta, -N_\Omega(z^k)) \leq \epsilon$, which only enlarges the feasible set. Any non-uniqueness present in ICO persists under regularization, and additional ambiguity may be introduced unless further structure, such as strong convexity, full-rank conditions, or explicit priors, is imposed. This motivates the alternative approaches developed in subsequent sections.

2.3. Sufficient Conditions for Parameter Identifiability

The non-identifiability results of Theorems 1–2 establish that parameter recovery is generically set-valued. We now provide sufficient conditions under which the inverse parameter becomes unique (up to normalization). These conditions directly address the two sources of ambiguity identified in Remark 3.

ASSUMPTION 4 (**Strong Convexity in Decision Variable**). *For every $\theta \in \Theta$, the function $x \mapsto f(x, \theta) = \sum_{j=1}^p \theta_j \phi_j(x)$ is μ -strongly convex on Ω for some $\mu > 0$ independent of θ .*

Strong convexity ensures that the forward problem $\mathcal{FO}(\theta, \Omega)$ admits a unique optimal solution $x^*(\theta)$ for each θ . This eliminates ambiguity in the forward direction but does not, by itself, guarantee identifiability of the inverse problem.

ASSUMPTION 5 (**One-Dimensional Normal Cones**). *For each imputed optimum z^k , the normal cone is one-dimensional: $N_\Omega(z^k) = \text{cone}\{n^k\}$, with $\|n^k\|_2 = 1$.*

Assumption 5 directly addresses the first source of non-identifiability from Proposition 2(ii): it rules out high-dimensional normal cones by requiring each z^k to lie on a smooth portion of the boundary $\partial\Omega$ where exactly one constraint is active, or more generally, where the active constraint normals are collinear.

ASSUMPTION 6 (Orthogonal Persistent Excitation). Let $A(z) := [\nabla\phi_1(z) \cdots \nabla\phi_p(z)] \in \mathbb{R}^{n \times p}$ denote the gradient matrix and $P_k := I_n - n^k(n^k)^\top$ the orthogonal projection onto the hyperplane perpendicular to n^k . The following excitation matrix is positive definite, $S \succ 0$:

$$S := \sum_{k=1}^K A(z^k)^\top P_k A(z^k) \in \mathbb{R}^{p \times p}.$$

Assumption 6 addresses the second source of non-identifiability from Proposition 4(i): it ensures that no nonzero parameter perturbation $\Delta\theta$ can produce gradient changes lying entirely along the normal directions $\{n^k\}$. The projection P_k extracts the component of $A(z^k)\Delta\theta$ orthogonal to n^k , and positive definiteness of S ensures this orthogonal component is nonzero for any $\Delta\theta \neq 0$.

REMARK 4. The matrix S measures how well the observations $\{z^k\}$ excite the parameter space in directions distinguishable from rescaling the dual multipliers. Consider the KKT condition $A(z^k)\theta = -\alpha_k n^k$ for some $\alpha_k \geq 0$. A perturbation $\theta \rightarrow \theta + \Delta\theta$ can be absorbed by adjusting $\alpha_k \rightarrow \alpha_k + \Delta\alpha_k$ if and only if $A(z^k)\Delta\theta$ is parallel to n^k . The condition $S \succ 0$ ensures that across all observations, no such hidden perturbation direction exists.

THEOREM 3 (Parameter Identifiability Under Orthogonal Excitation). Under Assumptions 4–6, and a normalization convention $\theta \in \Theta$ (e.g., $\|\theta\|_2 = 1$ with a sign convention, or $\mathbf{1}^\top \theta = 1$ with $\theta \geq 0$), the parameter θ solving \mathcal{ICO} is unique.

PROPOSITION 5 (Necessity of Orthogonal Excitation for Identifiability). Under Assumptions 4–5, if $S = \sum_{k=1}^K A(z^k)^\top P_k A(z^k)$ is singular, then there exist distinct parameters $\theta, \theta' \in \mathbb{R}^p$ (prior to normalization) that both satisfy the KKT conditions at all imputed optima $\{z^k\}_{k=1}^K$. Consequently, \mathcal{ICO} admits multiple solutions, and identifiability fails.

The null space of S characterizes the unidentifiable directions in parameter space: perturbations $\Delta\theta \in \ker(S)$ produce gradient changes $A(z^k)\Delta\theta$ that are entirely absorbed by adjusting the dual multipliers α_k . These directions are invisible to the inverse problem and represent fundamental limitations of the available data.

An alternative identifiability approach requires the stacked gradient matrix $\bar{A} := [A(z^1)^\top \cdots A(z^K)^\top]^\top \in \mathbb{R}^{Kn \times p}$ to have full column rank. This condition is neither necessary nor sufficient for identifiability: (i) *Not necessary:* Even if \bar{A} is rank-deficient, S may still be positive definite if the rank deficiency occurs along normal directions that are projected away. (ii) *Not sufficient:* Even if \bar{A} has full rank, parameter perturbations along normal directions can remain unidentifiable if $\dim(N_\Omega(z^k)) > 1$, violating Assumption 5. The orthogonal excitation condition precisely captures the identifiable information content of the data.

REMARK 5. The matrix $M := \sum_{k=1}^K A(z^k)^\top n^k (n^k)^\top A(z^k)$ captures alignment of gradient directions along the normals n^k . Note the decomposition $S + M = \sum_k A(z^k)^\top A(z^k)$, the standard Gramian. While M measures how well the data determine the dual multipliers α_k , it is S that governs parameter identifiability: $M \succ 0$ alone does not imply identifiability; $S \succ 0$ is both necessary and sufficient (under Assumptions 4–5); and the decomposition separates the Gramian into identifiable (S) and non-identifiable (M) components.

The positive definiteness of S may be difficult to verify a priori since it depends on the (unknown) imputed optima $\{z^k\}$. We provide simpler sufficient conditions.

COROLLARY 2 (Sufficient Conditions for Positive Definite S). *Assumption 6 ($S \succ 0$) is satisfied if either of the following holds:*

- (i) *The normal directions $\{n^k\}_{k=1}^K$ span \mathbb{R}^n , and for each k , $A(z^k)$ has full column rank p .*
- (ii) *At least one observation z^{k_0} lies in the interior of Ω (so $N_\Omega(z^{k_0}) = \{0\}$ and $P_{k_0} = I$), and $A(z^{k_0})$ has full column rank.*

Corollary 2(ii) indicates that identifiability is easiest to achieve when some observations correspond to interior optima. In constrained settings, condition (i) requires geometric diversity in the active constraints across observations, which is a form of experimental design for inverse optimization. When these conditions fail, the practitioner should expect set-valued parameter recovery and may employ the characterization methods developed in subsequent sections.

3. Inverse Learning: A Scalable Framework for Data-Rich Inverse Optimization

The classical formulations \mathcal{ICO} and $\mathcal{R-ICO}$ face two fundamental challenges in data-rich settings: (i) Computational intractability: \mathcal{ICO} requires $O(Kn + Km)$ variables and $O(Km)$ constraints. For modern applications with thousands of data points, this scaling renders classical formulations impractical. (ii) Inherent non-identifiability: Theorems 1–2 establish that parameter recovery is generically set-valued. Classical approaches either ignore this multiplicity (returning an arbitrary feasible θ) or require stringent conditions (Theorem 3) that are rarely satisfied in practice.

We propose *Inverse Learning* (\mathcal{IL}), which addresses both challenges through a fundamental reformulation: rather than imputing K separate optimal solutions $\{z^k\}_{k=1}^K$, \mathcal{IL} learns a *single representative optimal solution* $z^* \in \Omega$ that best fits the observed data. This approach targets settings where observations are noisy measurements of a common latent optimal decision—a natural assumption when a single decision-maker’s behavior is observed repeatedly under noise.

3.1. The Inverse Learning Formulation

Given observations $\mathcal{X} = \{x^k\}_{k=1}^K$ and feasible set Ω , the Inverse Learning problem seeks a single optimal solution z^* such that: (1) z^* minimizes the aggregate distance to observations; (2) z^* is optimal for $\mathcal{FO}(\theta, \Omega)$ for some $\theta \in \Theta$; and (3) the set of all compatible parameters $\Theta^*(z^*)$ is characterized. The \mathcal{IL} model can be written as follows:

$$\mathcal{IL}(\mathcal{X}, \Omega): \quad \min_{z, \theta, \lambda} \quad \sum_{k=1}^K \|x^k - z\|_2^2 \quad (8a)$$

$$\text{s.t.} \quad g_i(z) \leq 0, \quad i = 1, \dots, m, \quad (8b)$$

$$\sum_{j=1}^p \theta_j \nabla \phi_j(z) + \sum_{i=1}^m \lambda_i \nabla g_i(z) = 0, \quad (8c)$$

$$\lambda_i g_i(z) = 0, \quad i = 1, \dots, m, \quad (8d)$$

$$\lambda \geq 0, \quad \theta \in \Theta. \quad (8e)$$

The objective (8a) minimizes aggregate squared error. Constraint (8b) ensures primal feasibility. Constraints (8c)–(8e) encode the KKT conditions, ensuring z is optimal for some forward problem with parameters (θ, λ) .

THEOREM 4 (Complexity Reduction). *The problem $\mathcal{IL}(\mathcal{X}, \Omega)$ has $O(n + p + m)$ variables and $O(n + m)$ constraints, independent of the number of observations K . In contrast, $\mathcal{ICO}(\mathcal{X}, \Omega)$ has $O(Kn + p + Km)$ variables and $O(Kn + Km)$ constraints.*

Theorem 4 establishes *data scalability*: the problem size is independent of K (See Table 1 for summary comparison). However, \mathcal{IL} remains nonconvex due to bilinear terms in (8c) and complementarity constraints (8d). The computational advantage lies in the ability to process arbitrarily large datasets through aggregated statistics (Proposition 6) and problem size reduction independent of K , not in polynomial-time solvability. For the linear case with polyhedral Ω , complementarity can be handled via mixed-integer programming with $O(m)$ binary variables, independent of K .

PROPOSITION 6 (Data Aggregation Property). *The objective function satisfies*

$$\sum_{k=1}^K \|x^k - z\|_2^2 = K \|z - \bar{x}\|_2^2 + \sum_{k=1}^K \|x^k - \bar{x}\|_2^2, \quad (9)$$

where $\bar{x} = \frac{1}{K} \sum_{k=1}^K x^k$ is the sample centroid. Consequently, $\mathcal{IL}(\mathcal{X}, \Omega)$ is equivalent to

$$\min_{z, \theta, \lambda} \quad K \|z - \bar{x}\|_2^2 \quad \text{s.t.} \quad (8b) \text{--}(8e), \quad (10)$$

which depends on the data only through the centroid \bar{x} .

The reduction (9) is specific to squared Euclidean loss. For ℓ_1 loss, the analogous aggregation uses the componentwise median. For general ℓ_p losses with $p \neq 1, 2$, no finite-dimensional aggregation exists, and the solver must retain all K data points. The scalability of \mathcal{IL} via aggregation is thus loss-dependent, though the constraint-side complexity reduction (Theorem 4) holds universally. The aggregation property enables: (i) Streaming updates: $\bar{x}_{K+1} = \frac{K}{K+1}\bar{x}_K + \frac{1}{K+1}x^{K+1}$; (ii) Parallelization: partial centroids from data partitions can be combined via weighted averaging; and (iii) Memory efficiency: only $\bar{x} \in \mathbb{R}^n$ need be stored, not the full dataset $\mathcal{X} \in \mathbb{R}^{n \times K}$.

3.2. Characterization of \mathcal{IL} Properties

Unlike classical IO, which returns a single (often arbitrary) feasible parameter, \mathcal{IL} explicitly characterizes all compatible parameters. Under Assumption 2, the KKT conditions are necessary and sufficient for optimality, and the normal cone admits the representation

$$N_{\Omega}(z) = \left\{ \sum_{i \in I(z)} \mu_i \nabla g_i(z) : \mu_i \geq 0 \right\} = \text{cone}\{\nabla g_i(z) : i \in I(z)\}, \quad (11)$$

where $I(z) = \{i : g_i(z) = 0\}$ is the active set.

THEOREM 5 (Parameter Set Characterization). *Let $(z^*, \theta^*, \lambda^*)$ solve $\mathcal{IL}(\mathcal{X}, \Omega)$. Define the active set $I(z^*) = \{i : g_i(z^*) = 0\}$. Under Assumption 2, the set of all parameters for which z^* is optimal is*

$$\Theta^*(z^*) = \{\theta \in \Theta : A(z^*)\theta \in -N_{\Omega}(z^*)\}, \quad (12)$$

where $A(z^*) = [\nabla \phi_1(z^*) \cdots \nabla \phi_p(z^*)]$ and $N_{\Omega}(z^*)$ is given by (11).

For the linear case, \mathcal{IL} admits a geometric characterization that clarifies its structure.

ASSUMPTION 7 (Regularity for Consistency). *The following conditions hold: (i) Θ is compact and the mapping $(z, \theta) \mapsto A(z)\theta$ is continuous; (ii) the feasible region Ω is closed and convex; (iii) the true solution z_0 lies in the relative interior of a face F_0 of \mathcal{Z}^* ; and (iv) there exists a neighborhood \mathcal{U} of z_0 such that $\mathcal{Z}^* \cap \mathcal{U} = F_0 \cap \mathcal{U}$, where F_0 is a closed convex set.*

PROPOSITION 7 (Geometric Interpretation for Linear \mathcal{IL}). *Consider the linear case with $\phi_j(x) = x_j$ and polyhedral $\Omega = \{x : Ax \geq b\}$. Let $\mathcal{Z}^* = \{z \in \Omega : \exists \theta \in \Theta \text{ such that } z \in \arg \min_{x \in \Omega} \theta^\top x\}$ be the set of points that can be made optimal for some θ . Under Assumption 7(iv), in a neighborhood \mathcal{U} of \bar{x} where $\mathcal{Z}^* \cap \mathcal{U}$ coincides with a single convex face F , the \mathcal{IL} solution satisfies $z_{\mathcal{IL}}^* = \arg \min_{z \in F} \|z - \bar{x}\|_2^2 = \text{proj}_F(\bar{x})$, i.e., $z_{\mathcal{IL}}^*$ is the projection of the data centroid onto the locally active face.*

To establish the statistical properties of the Inverse Learning framework, we first formalize the data-generating process. We assume that the observed data represent noisy deviations around a single latent optimal decision.

ASSUMPTION 8 (Data Generating Process). *Observations are generated as $x^k = z_0 + \xi^k$, where $z_0 \in \Omega$ is optimal for $\mathcal{FO}(\theta_0, \Omega)$ for some true parameter $\theta_0 \in \Theta$, and $\{\xi^k\}_{k=1}^K$ are i.i.d. random vectors with $\mathbb{E}[\xi^k] = 0$ and $\mathbb{E}[\|\xi^k\|_2^2] = \sigma^2 < \infty$.*

Under this noise model, we can establish the asymptotic consistency of the \mathcal{IL} estimator. Specifically, as the sample size grows, the recovered solution almost surely converges to the true latent optimum, and the recovered parameter set correctly bounds the compatible true parameters.

THEOREM 6 (Consistency of Inverse Learning). *Under Assumptions 2, 7, and 8, as $K \rightarrow \infty$:*

- (i) $\bar{x} \xrightarrow{a.s.} z_0$.
- (ii) $z_{\mathcal{IL}}^* \xrightarrow{a.s.} z_0$.
- (iii) *The parameter set mapping is outer semicontinuous: $\limsup_{K \rightarrow \infty} \Theta^*(z_{\mathcal{IL}}^*) \subseteq \Theta^*(z_0)$.*

Beyond asymptotic consistency, the centroid aggregation property of the \mathcal{IL} framework also imparts a natural degree of finite-sample robustness against anomalous observations, provided the structural neighborhood is preserved.

PROPOSITION 8 (Robustness to Outliers). *Let $\mathcal{X}_{out} = \mathcal{X} \cup \{x_{out}\}$ where $\|x_{out} - \bar{x}\|_2 = R$. Under Assumption 7(iv), if the corrupted centroid $\bar{x}_{out} = \frac{K\bar{x} + x_{out}}{K+1}$ remains in \mathcal{U} , then $\|z_{out}^* - z_{\mathcal{IL}}^*\|_2 \leq \|\bar{x}_{out} - \bar{x}\|_2 = R/(K+1)$.*

3.3. Identifiability of Inverse Learning

We establish the central theoretical contribution: \mathcal{IL} achieves *solution identifiability* under conditions that differ from—and are in many cases less restrictive than—those required by classical \mathcal{IO} for *parameter identifiability*. Classical inverse optimization seeks to identify the true parameter θ_0 , which requires one-dimensional normal cones (Assumption 5) and orthogonal persistent excitation $S \succ 0$ (Assumption 6). These conditions are restrictive. Inverse Learning instead focuses on identifying the *true optimal solution* z_0 rather than the parameter θ_0 , enabling identifiability under different conditions.

DEFINITION 1 (SOLUTION IDENTIFIABILITY). The inverse problem is *solution-identifiable* if the optimal solution z^* is uniquely determined by the data \mathcal{X} , even when multiple parameters $\theta \in \Theta^*(z^*)$ are compatible with z^* .

Inverse Learning uniquely pinpoints the true optimal solution, provided the optimality set is sufficiently well-behaved in the neighborhood of that solution.

THEOREM 7 (Solution Identifiability of \mathcal{IL}). *Under Assumptions 2 and 7, the \mathcal{IL} solution $z_{\mathcal{IL}}^*$ is unique. Moreover, $z_{\mathcal{IL}}^*$ is consistently estimable: $z_{\mathcal{IL}}^* \xrightarrow{a.s.} z_0$ as $K \rightarrow \infty$ under Assumption 8.*

Table 2 summarizes the divergent requirements for classical \mathcal{IO} versus \mathcal{IL} . The following proposition explicitly details why these two sets of conditions are mathematically incomparable.

PROPOSITION 9 (IL Achieves Solution Identifiability Under Different Conditions). *The conditions for solution identifiability in \mathcal{IL} (Assumption 7) differ from those for parameter identifiability in classical \mathcal{IO} (Assumptions 5–6) as follows:*

- (i) \mathcal{IL} does not require one-dimensional normal cones. The solution $z_{\mathcal{IL}}^*$ can lie at a vertex where multiple constraints are active.
- (ii) \mathcal{IL} does not require orthogonal excitation. The gradient matrix $A(z)$ need not satisfy any rank condition for solution uniqueness.
- (iii) \mathcal{IL} requires local convexity of the optimality set \mathcal{Z}^* near the true solution (Assumption 7(iv)), a condition not needed by classical \mathcal{IO} .

The two sets of conditions are thus incomparable: neither strictly implies the other.

Although \mathcal{IL} does not require parameter identifiability, it can achieve it under the same conditions as classical \mathcal{IO} .

COROLLARY 3 (Parameter Identifiability via \mathcal{IL}). *If the conditions of Theorem 3 hold (Assumptions 4–6), then $\Theta^*(z_{\mathcal{IL}}^*)$ is a singleton, and \mathcal{IL} recovers the unique true parameter θ_0 (up to normalization).*

When parameter identifiability fails, \mathcal{IL} provides explicit characterization of the admissible parameter set.

PROPOSITION 10 (Structure of $\Theta^*(z^*)$). *The set $\Theta^*(z^*) = \{\theta \in \Theta : A(z^*)\theta \in -N_{\Omega}(z^*)\}$ has the following structure:*

- (i) *General case: $\Theta^*(z^*)$ is the intersection of Θ with the preimage of the cone $-N_{\Omega}(z^*)$ under the linear map $\theta \mapsto A(z^*)\theta$. This set is convex.*
- (ii) *Polyhedral case: If Ω is polyhedral, then $N_{\Omega}(z^*)$ is a polyhedral cone, and $\Theta^*(z^*)$ is a convex polyhedron.*
- (iii) *One-dimensional normal cone: If $N_{\Omega}(z^*) = \text{cone}\{n^*\}$ for some $n^* \in \mathbb{R}^n$, then $\Theta^*(z^*) = \{\theta \in \Theta : A(z^*)\theta = -\alpha n^* \text{ for some } \alpha \geq 0\}$, and $\dim(\Theta^*(z^*) \cap \{\theta : \|\theta\|_2 = 1\}) = p - 1 - \text{rank}(P_{n^*}A(z^*))$, where $P_{n^*} = I - n^*(n^*)^\top$ projects orthogonally to n^* .*

Inverse Learning provides a computationally scalable and theoretically rigorous framework for inverse optimization in data-rich settings, where observations represent noisy measurements of

a common latent optimal decision. Its key properties are: (1) Data scalability: Problem size is $O(n + m + p)$, independent of K , with data entering only through the centroid \bar{x} . (2) Explicit non-uniqueness handling: \mathcal{IL} returns the full parameter set $\Theta^*(z^*)$, making ambiguity explicit. (3) Statistical guarantees: Consistency holds under standard regularity assumptions. (4) Solution identifiability: The optimal solution z^* is uniquely identified under conditions that do not require parameter identifiability.

IL and classical \mathcal{ICO} address different modeling scenarios: \mathcal{IL} assumes a single latent optimal solution observed with noise, while \mathcal{ICO} allows heterogeneous behavior across observations. The next section extends this framework to address the tradeoff between fidelity to observations and adherence to domain-specific constraints.

4. Goal-Integrated Inverse Learning: Navigating the Observation-Constraint Tradeoff

The \mathcal{IL} framework provides a computationally efficient approach to learning optimal solutions from observed data. However, a fundamental tension emerges in many applications: the solution $z_{\mathcal{IL}}^*$ that best fits observed behaviors may not adequately reflect expert-defined constraints or organizational goals. In healthcare contexts such as dietary management, a patient's observed food intake may systematically deviate from nutritional guidelines encoded in the constraints. While \mathcal{IL} recovers a solution optimal for *some* objective function, Theorem 5 establishes that this solution typically activates only a minimal set of constraints.

This section develops the *Goal-Integrated Inverse Learning (GIL)* framework, providing decision-makers with explicit mechanisms to navigate the tradeoff between observational fidelity and constraint satisfaction. We introduce two complementary models: \mathcal{GIL} (Section 4.1) controls the exact number r of binding relevant constraints, enabling systematic exploration of the tradeoff spectrum; and *Modified GIL (MGIL)* (Section 4.2) provides structured sequential navigation by iteratively adding constraints while maintaining all previously active ones.

DEFINITION 2 (OBSERVATION-CONSTRAINT TRADEOFF). Let $z_{\text{proj}} := \arg \min_{z \in \Omega} \sum_{k=1}^K \|x^k - z\|_2^2$ be the projection of observed data onto the feasible region (ignoring forward-optimality structure), and let $z_{\text{goal}} \in \Omega$ be a solution binding a maximal set of expert-defined constraints. The *Observation-Constraint Tradeoff* is the spectrum of solutions that balance observational fidelity against constraint satisfaction, parameterized by the number and type of active constraints.

ASSUMPTION 9 (Constraint Hierarchy). *The constraint index set $\{1, \dots, m\}$ admits a partition into three disjoint subsets: (i) Relevant Constraints \mathcal{R} : constraints representing expert knowledge or goals that may not all be simultaneously active in practice; (ii) Preferred Constraints $\mathcal{P} \subseteq \mathcal{R}$: a subset*

deemed particularly important by domain experts; and (iii) Trivial Constraints $\mathcal{T} = \{1, \dots, m\} \setminus \mathcal{R}$: constraints necessary for well-posedness (e.g., non-negativity) but not of primary interest. We assume that for each $r \in \{1, \dots, n\}$, there exist subsets of \mathcal{R} of size r whose constraint gradients are linearly independent at relevant feasible points (a local LICQ-type condition).

If no domain knowledge distinguishes constraint importance, set $\mathcal{R} = \{1, \dots, m\}$, $\mathcal{P} = \emptyset$, and $\mathcal{T} = \emptyset$. The framework reduces to standard \mathcal{IL} in limiting cases.

4.1. Goal-Integrated Inverse Learning (GIL)

GIL provides direct control over the number of binding relevant constraints through a cardinality parameter $r \in \{1, \dots, n\}$.

$$\text{GIL}(\mathcal{X}, \Omega, \mathcal{R}, \mathcal{P}, r, \omega) : \quad \min_{z, \theta, \lambda, v} \quad \omega \sum_{k=1}^K \|x^k - z\|_2^2 - (1 - \omega) \sum_{i \in \mathcal{P}} v_i \quad (13a)$$

$$\text{s.t.} \quad \sum_{j=1}^p \theta_j \nabla \phi_j(z) + \sum_{i=1}^m \lambda_i \nabla g_i(z) = 0, \quad (13b)$$

$$g_i(z) \leq 0, \quad \forall i \in \{1, \dots, m\}, \quad (13c)$$

$$\lambda_i \leq M v_i, \quad \forall i \in \{1, \dots, m\}, \quad (13d)$$

$$g_i(z) \leq -\varepsilon(1 - v_i), \quad \forall i \in \mathcal{R}, \quad (13e)$$

$$v_i = 1 \Rightarrow g_i(z) = 0, \quad \forall i \in \{1, \dots, m\}, \quad (13f)$$

$$v_i \in \{0, 1\}, \quad \forall i \in \{1, \dots, m\}, \quad (13g)$$

$$\sum_{i \in \mathcal{R}} v_i = r, \quad (13h)$$

$$\lambda \geq 0, \quad \theta \in \Theta, \quad (13i)$$

where $M > 0$ is a sufficiently large constant (see Remark 6), $\varepsilon > 0$ is a small slack parameter ensuring inactive relevant constraints are strictly slack, $\omega \in [0, 1]$ controls the tradeoff weight, and $v_i \in \{0, 1\}$ indicates whether constraint i is selected as active.

REMARK 6. Constraint (13f) can be linearized as $-g_i(z) \leq M(1 - v_i)$ for sufficiently large M . We assume M is chosen as a valid upper bound satisfying $M \geq \max\{\lambda_i^* : (z^*, \theta^*, \lambda^*) \text{ is KKT-optimal for some } \theta \in \Theta\}$ and $M \geq \max_{z \in \Omega} |g_i(z)|$ for all i . Modern MIP solvers (Gurobi, CPLEX) support *indicator constraints* directly (e.g., $v_i = 0 \Rightarrow \lambda_i = 0$ and $v_i = 1 \Rightarrow g_i(z) = 0$), which are numerically more stable and avoid specifying explicit bounds.

REMARK 7. Constraints (13d)–(13f) enforce a chosen complementarity pattern: $v_i = 0$ forces $\lambda_i = 0$ and $g_i(z) \leq -\varepsilon$ (strictly slack for $i \in \mathcal{R}$), while $v_i = 1$ forces $g_i(z) = 0$ (active) and allows $\lambda_i \in [0, M]$. Combined with stationarity (13b), primal feasibility (13c), and dual feasibility (13i), any

feasible solution satisfies the KKT conditions for some forward problem. Under Assumption 2, KKT conditions are sufficient for optimality, so each feasible (z, θ, λ, v) corresponds to a point z that is forward-optimal for parameter θ .

The slack constraint (13e) ensures that for $i \in \mathcal{R}$ with $v_i = 0$, we have $g_i(z) \leq -\varepsilon < 0$, so the constraint is *strictly* inactive. This prevents accidental activation where $g_i(z) = 0$ but $v_i = 0$, ensuring (13h) guarantees *exactly* r relevant constraints are binding. Note that for trivial constraints $i \in \mathcal{T}$, no slack enforcement applies; these may be incidentally active regardless of their v_i value.

4.1.1. Theoretical Properties of \mathcal{GIL} We begin by establishing the computational complexity of the \mathcal{GIL} formulation. Like the base Inverse Learning model, \mathcal{GIL} preserves the critical property of sample-size independence.

PROPOSITION 11 (\mathcal{GIL} Complexity). *\mathcal{GIL} has $O(n + p + m)$ continuous variables, m binary variables, and $O(m)$ constraints—all independent of K . The objective depends on data only through $\bar{x} = \frac{1}{K} \sum_k x^k$.*

In order to ensure the user-specified constraint cardinality is actually attainable within the problem geometry, a standard realizability condition is required.

ASSUMPTION 10 (Realizability). *For the given cardinality r , there exists at least one point $z \in \Omega$ such that: (i) exactly r relevant constraints are active: $|\{i \in \mathcal{R} : g_i(z) = 0\}| = r$; (ii) the remaining relevant constraints satisfy $g_i(z) < 0$; (iii) the gradients of the active constraints are linearly independent at z (LICQ); and (iv) there exist (θ, λ) satisfying stationarity (13b) with $\theta \in \Theta$ and $\lambda \geq 0$.*

We can formally guarantee that \mathcal{GIL} is well-posed and yields a solution that is optimal for the forward problem.

THEOREM 8 (\mathcal{GIL} Feasibility and Optimality). *Under Assumptions 2, 9, and 10, and if Ω is non-empty and compact, then: (a) the feasible set of \mathcal{GIL} is non-empty; (b) an optimal solution $(z^*, \theta^*, \lambda^*, v^*)$ exists; and (c) the solution z^* is optimal for $\mathcal{FO}(\theta^*, \Omega)$.*

Similar to the Inverse Learning model, \mathcal{GIL} provides an explicit mathematical boundary for all parameters compatible with the forced constraint activation pattern.

THEOREM 9 (\mathcal{GIL} Parameter Set Characterization). *Let $(z^*, \theta^*, \lambda^*, v^*)$ solve \mathcal{GIL} . Define the active set $\mathcal{A}(z^*) := \{i : g_i(z^*) = 0\}$. Under the slack enforcement (13e), $\mathcal{A}(z^*) \cap \mathcal{R} = \{i \in \mathcal{R} : v_i^* = 1\}$. The set of all parameters for which z^* is optimal is:*

$$\Theta^*(z^*) = \{\theta \in \Theta : A(z^*)\theta \in -N_\Omega(z^*)\}, \quad (14)$$

where $N_\Omega(z^*) = \text{cone}\{\nabla g_i(z^*) : i \in \mathcal{A}(z^*)\}$ under Assumption 2.

GIL does **not** guarantee monotone increase of $D_r := \sum_k \|x^k - z_r^*\|_2^2$ with r . The feasible sets for different r values are disjoint (not nested), so optimal values cannot be compared via containment arguments. Practitioners should solve \mathcal{GIL} for a range of r values to characterize the tradeoff empirically. As such, we also consider the Modified Goal-Integrated Inverse Learning in the following.

4.2. Modified Goal-Integrated Inverse Learning (\mathcal{MGIL})

While \mathcal{GIL} explores the tradeoff by varying r , solutions for different r may lie on entirely different faces of Ω . \mathcal{MGIL} provides a *structured sequential path*: each iteration adds at least one new binding constraint while maintaining all previously active ones. Given a seed solution $z_{\text{prev}} \in \Omega$ with active set $\mathcal{A}_{\text{prev}} = \{i \in \mathcal{R} : g_i(z_{\text{prev}}) = 0\}$:

$$\mathcal{MGIL}(\mathcal{X}, \Omega, \mathcal{R}, \mathcal{P}, z_{\text{prev}}, \omega) : \min_{z, \theta, \lambda, v} \omega \sum_{k=1}^K \|x^k - z\|_2^2 - (1 - \omega) \sum_{i \in \mathcal{P}} v_i \quad (15a)$$

$$\text{s.t.} \quad \sum_{j=1}^p \theta_j \nabla \phi_j(z) + \sum_{i=1}^m \lambda_i \nabla g_i(z) = 0, \quad (15b)$$

$$g_i(z) \leq 0, \quad \forall i \in \{1, \dots, m\}, \quad (15c)$$

$$g_i(z) = 0, \quad \forall i \in \mathcal{A}_{\text{prev}}, \quad (15d)$$

$$\lambda_i \leq M v_i, \quad \forall i \in \{1, \dots, m\}, \quad (15e)$$

$$g_i(z) \leq -\varepsilon(1 - v_i), \quad \forall i \in \mathcal{R} \setminus \mathcal{A}_{\text{prev}}, \quad (15f)$$

$$v_i = 1 \Rightarrow g_i(z) = 0, \quad \forall i \in \{1, \dots, m\}, \quad (15g)$$

$$v_i \in \{0, 1\}, \quad \forall i \in \{1, \dots, m\}, \quad (15h)$$

$$\sum_{i \in \mathcal{R} \setminus \mathcal{A}_{\text{prev}}} v_i \geq 1, \quad (15i)$$

$$\lambda \geq 0, \quad \theta \in \Theta. \quad (15j)$$

Two constraints distinguish \mathcal{MGIL} from \mathcal{GIL} : (i) Inheritance (15d) forces all constraints active at z_{prev} to remain active, ensuring solutions lie on nested faces; and (ii) Increment (15i) requires at least one new relevant constraint to bind, creating a structured path $z_0 \rightarrow z_1 \rightarrow z_2 \rightarrow \dots$ of increasing constraint satisfaction. The following theorems provide the main theoretical properties of \mathcal{MGIL} .

THEOREM 10 (Monotone Distance Sequence). *Let $\{z_\ell\}_{\ell=0}^L$ be generated by iteratively solving \mathcal{MGIL} with $\omega = 1$ and $\mathcal{P} = \emptyset$, starting from z_0 . Define $D_\ell := \sum_{k=1}^K \|x^k - z_\ell\|_2^2$. Then $D_0 \leq D_1 \leq D_2 \leq \dots \leq D_L$.*

This monotonic increase in distance is a direct consequence of the underlying problem geometry. By iteratively adding binding constraints while maintaining all previously active ones, \mathcal{MGIL} restricts the optimization to a sequence of progressively lower-dimensional, nested faces of the feasible region.

THEOREM 11 (Face Containment). *For a sequence $\{z_\ell\}_{\ell=0}^L$ generated by \mathcal{MGIL} , define $\mathcal{F}_\ell := \{z \in \Omega : g_i(z) = 0, \forall i \in \mathcal{A}_\ell\}$, where $\mathcal{A}_\ell = \{i : g_i(z_\ell) = 0\}$. Then $\mathcal{F}_0 \supseteq \mathcal{F}_1 \supseteq \dots \supseteq \mathcal{F}_L$ and $z_\ell \in \mathcal{F}_\ell$ for all ℓ .*

A powerful theoretical benefit of this nested geometric structure is that parameter compatibility is partially preserved along the sequential path. Specifically, for linear programs, the constant objective gradients mean that any parameter vector rationalizing an earlier solution remains structurally valid for all subsequent solutions in the sequence.

THEOREM 12 (Persistent Optimality (Linear Case)). *Assume $f(x, \theta) = \theta^\top x$ with $p = n$ and $\phi_j(x) = x_j$ (linear objective). Let $\{z_\ell\}_{\ell=0}^L$ be generated by \mathcal{MGIL} . For any $\ell' \in \{0, \dots, L\}$ and any $\ell \leq \ell'$, the solution $z_{\ell'}$ is optimal for $\mathcal{FO}(\theta, \Omega)$ for any $\theta \in \text{cone}\{a_i : i \in \mathcal{A}_\ell\} \cap \Theta$, where a_i are the constraint normals.*

For general convex objectives where $A(z)$ depends on z , the persistent optimality statement requires modification. The normal cone $N_\Omega(z_{\ell'})$ contains the cone generated by inherited constraint gradients, ensuring existence of *some* $\theta \in \Theta$ making $z_{\ell'}$ optimal, but this θ may differ from parameters supporting earlier solutions.

COROLLARY 4 (Structured Tradeoff Quantification). *The sequence $\{z_\ell, D_\ell, \Theta^*(z_\ell)\}_{\ell=0}^L$ characterizes the observation-constraint tradeoff: each step reveals the marginal cost $\Delta D_\ell = D_{\ell+1} - D_\ell \geq 0$ of activating additional constraints.*

THEOREM 13 (\mathcal{MGIL} Consistency). *Under Assumptions 2, 8, and 7, let $\{z_\ell^0\}_{\ell=0}^{L_0}$ be the population sequence (infinite data) and $\{z_\ell^K\}_{\ell=0}^{L_K}$ the finite-sample sequence. For any fixed ℓ : $z_\ell^K \xrightarrow{P} z_\ell^0$ as $K \rightarrow \infty$.*

Algorithm 1 operationalizes the observation-constraint tradeoff. The procedure is initialized by solving the base \mathcal{IL} model to anchor the sequence at the point of maximum observational fidelity (z_0). At each iteration, the algorithm tightens the feasible region by solving the \mathcal{MGIL} formulation, forcing at least one additional relevant constraint to bind while strictly inheriting all previously active ones. The algorithm introduces a user-defined marginal cost threshold (τ). If the degradation in observational fit ($D_{\ell+1} - D_\ell$) required to satisfy the next constraint exceeds this tolerance, the sequential path terminates. This yields a structured, reliable menu of decision options that explicitly maps the cost of adherence. We next theorize the relationship between \mathcal{GIL} and \mathcal{MGIL} .

4.3. Relationship Between \mathcal{GIL} and \mathcal{MGIL}

Let z_0 be the \mathcal{IL} solution with $|\mathcal{A}_0| = r_0$ active relevant constraints. (a) \mathcal{GIL} with $r = r_0 + k$ explores solutions binding exactly $r_0 + k$ relevant constraints, but these may lie on any face satisfying the

Algorithm 1 Modified Goal-Integrated Inverse Learning (MGIL)

Require: Observations \mathcal{X} , constraint sets \mathcal{R}, \mathcal{P} , region Ω , max iterations L_{\max} , weight ω , threshold

τ

Ensure: Sequence $\{z_\ell, \theta_\ell, D_\ell, \mathcal{A}_\ell\}_{\ell=0}^L$

- 1: Solve $\mathcal{IL}(\mathcal{X}, \Omega)$ to obtain z_0, θ_0
 - 2: $\mathcal{A}_0 \leftarrow \{i \in \mathcal{R} : g_i(z_0) = 0\}$; $D_0 \leftarrow \sum_k \|x^k - z_0\|_2^2$; $\ell \leftarrow 0$
 - 3: **while** $\ell < L_{\max}$ **and** $|\mathcal{A}_\ell| < \min(|\mathcal{R}|, n)$ **do**
 - 4: Solve $\mathcal{MGIL}(\mathcal{X}, \Omega, \mathcal{R}, \mathcal{P}, z_\ell, \omega)$ to obtain $(z_{\ell+1}, \theta_{\ell+1}, \lambda_{\ell+1}, v_{\ell+1})$
 - 5: $\mathcal{A}_{\ell+1} \leftarrow \{i : g_i(z_{\ell+1}) = 0\}$; $D_{\ell+1} \leftarrow \sum_k \|x^k - z_{\ell+1}\|_2^2$
 - 6: **if** $D_{\ell+1} - D_\ell > \tau$ **then**
 - 7: **break** {Marginal cost exceeds threshold}
 - 8: **end if**
 - 9: $\ell \leftarrow \ell + 1$
 - 10: **end while**
 - 11: **return** $\{z_\ell, \theta_\ell, D_\ell, \mathcal{A}_\ell\}_{\ell=0}^L$
-

cardinality requirement. Different r values yield solutions on potentially disconnected faces. (b) \mathcal{MGIL} iterated k times from z_0 yields $\{z_\ell\}_{\ell=1}^k$ with $|\mathcal{A}_\ell| \geq r_0 + \ell$, and all solutions lie on nested faces: $z_\ell \in \mathcal{F}_\ell \subseteq \mathcal{F}_{\ell-1}$. It is best to *use \mathcal{GIL} when:* exploring qualitatively different solutions across the tradeoff, a specific target r is known, or parallel computation is available. *Use \mathcal{MGIL} when:* incremental adjustments are needed, marginal cost quantification is important, or consistency with an initial solution is required.

4.4. Parameter Selection from the Cone

Both \mathcal{GIL} and \mathcal{MGIL} characterize the full parameter set $\Theta^*(z^*)$. When a single representative is needed:

DEFINITION 3 (OBSERVATION-ALIGNED PARAMETER). Given solution z^* with active set $\mathcal{A}(z^*)$, the observation-aligned parameter is:

$$\theta^* \in \arg \min_{\theta \in \Theta^*(z^*)} \sum_{k=1}^K f(x^k, \theta).$$

For linear $f(x, \theta) = \theta^\top x$, this reduces to $\theta^* \in \arg \min_{\theta \in \Theta^*(z^*)} \theta^\top \bar{x}$: the parameter assigning lowest cost to average observed behavior.

4.5. Comparison with Classical Inverse Optimization

Under comparable conditions, the \mathcal{GIL} approach inherently dominates the traditional “recover-then-optimize” pipeline in terms of data fidelity.

THEOREM 14 (Dominance Over Recover-then-Optimize). *Let θ^{ICO} be recovered from classical \mathcal{ICO} , and let $z^{FO} \in \arg \min_{x \in \Omega} f(x, \theta^{ICO})$. Suppose z^{FO} satisfies Assumption 10 with $r = |\mathcal{A}(z^{FO}) \cap \mathcal{R}|$, i.e., z^{FO} is feasible for \mathcal{GIL} with this cardinality. Let $z_{\mathcal{GIL}}^*$ solve \mathcal{GIL} with the same r , $\omega = 1$, and $\mathcal{P} = \emptyset$. Then: $\sum_{k=1}^K \|x^k - z_{\mathcal{GIL}}^*\|_2^2 \leq \sum_{k=1}^K \|x^k - z^{FO}\|_2^2$.*

Theorem 14 establishes that when the recover-then-optimize solution is compatible with \mathcal{GIL} 's feasibility structure, \mathcal{GIL} provides equal or better observational fit while maintaining the same constraint satisfaction level. The conditioning reflects that forward-optimal solutions may have accidental activity patterns (e.g., constraints that are active but not strictly slack away from the boundary) that violate \mathcal{GIL} 's exact cardinality and strict slack requirements.

PROPOSITION 12 (Scalability).

<i>Model</i>	<i>Continuous Vars</i>	<i>Binary Vars</i>	<i>Dependence on K</i>
\mathcal{ICO}	$O(Kn + Km)$	0	Linear
\mathcal{IL}	$O(n + m)$	0	None
$\mathcal{GIL} / \mathcal{MGIL}$	$O(n + m)$	m	None

The Goal-Integrated Inverse Learning framework provides principled mechanisms to navigate the observation-constraint tradeoff: (1) \mathcal{GIL} enables direct control over constraint satisfaction level via cardinality parameter r , supporting parallel exploration without monotonicity guarantees. (2) \mathcal{MGIL} enables sequential navigation with guaranteed monotonicity (Theorem 10) and nested face structure (Theorem 11), providing interpretable marginal costs for each additional constraint. (3) Both maintain K -independence, enforce complete complementarity patterns (yielding forward-optimal solutions under Slater's condition), and characterize full parameter sets $\Theta^*(z^*)$. The choice between \mathcal{GIL} and \mathcal{MGIL} depends on application requirements: \mathcal{GIL} for broad exploration, \mathcal{MGIL} for incremental, interpretable transitions.

5. Numerical Experiments

We evaluate the proposed Inverse Learning framework, specifically \mathcal{IL} (8), \mathcal{GIL} (13), and \mathcal{MGIL} (15), against the classical inverse linear optimization benchmark (\mathcal{ILO}) (4). The experiments are designed to assess three dimensions of performance: (i) solution accuracy (proximity to the true optimal solution), (ii) parameter recovery rates (correct identification of the true cost vector cone), and (iii) computational efficiency, under controlled conditions across varying noise levels and constraint binding configurations.

5.1. Experimental Design

Instance Generation. We generate random linear programming instances in \mathbb{R}^n with $n = 10$. For each instance, a polyhedral feasible set $\Omega = \{x \in \mathbb{R}^n : Ax \geq b, x \geq 0\}$ is constructed with randomly generated constraint matrices, ensuring full-dimensional and non-empty feasible regions. Decision variables are bounded in $[-10, 10]^n$. Following Assumption 9, the non-negativity constraints form the trivial set \mathcal{T} , while the structural constraints $Ax \geq b$ constitute the relevant set \mathcal{R} .

Data Generation. The \mathcal{IL} framework and classical \mathcal{IO} rest on distinct modeling assumptions regarding the data-generating process. To provide a fair evaluation, we employ two data generation procedures, illustrated in Figure 2.

1. *IL Assumption Scenario* (consistent with Assumption 8): A true optimal solution $x^* \in \Omega$ is randomly selected from the boundary of Ω associated with relevant constraints. A corresponding true parameter vector θ^* is determined such that x^* is optimal for $\mathcal{FO}(\theta^*, \Omega)$; note that θ^* need not be unique (Theorem 1). Observations $\mathcal{X} = \{x^k\}_{k=1}^K$ (with K randomly chosen between 2 and 8) are generated as $x^k = x^* + \xi^k$, where $\xi^k \sim \mathcal{N}(0, \sigma^2 I)$.
2. *IO Assumption Scenario* (the classical \mathcal{IO} setting): A true parameter vector θ^* is randomly generated. The forward problem $\mathcal{FO}(\theta^*, \Omega)$ is solved to find the optimal set $\Omega^{opt}(\theta^*)$. K points $\{x_k^*\}_{k=1}^K$ are sampled from $\Omega^{opt}(\theta^*)$ (or the unique optimum is repeated K times if the optimal face is a singleton). Observations are generated by adding noise: $x^k = x_k^* + \xi^k$, where $\xi^k \sim \mathcal{N}(0, \sigma^2 I)$.

For both scenarios, three noise levels corresponding to standard deviations σ of 0%, 5%, and 20% relative to the diameter of the feasible set are tested. Observations may lie inside or outside Ω .

Models and Parameters. We solve \mathcal{IL} , \mathcal{ILCO} , \mathcal{GIL} , and \mathcal{MGIL} for each generated instance. For \mathcal{GIL} and \mathcal{MGIL} , we vary the cardinality parameter $r \in \{1, 2, \dots, 10\}$ (Section 4.1) and consider configurations both with and without randomly designated preferred constraints \mathcal{P} (Assumption 9). We also vary the “knowledge level”—that is, the number of true binding constraints known a priori—across values $\{1, 5, 10\}$ to test robustness to varying degrees of structural information.

Performance Metrics. We evaluate performance using three metrics:

Solution Distance. The ℓ_2 -norm distance between the learned solution (z^* for \mathcal{IL} models; z_{IO} obtained by solving \mathcal{FO} with the recovered θ_{IO}) and the true optimal solution.

Parameter Recovery Rate. Since parameters are generically non-unique (Theorems 1–2), we define recovery success as the event that the true parameter θ^* lies within the *cone* of parameters compatible with the recovered solution. For $\mathcal{GIL}/\mathcal{MGIL}$, this is $\Theta^*(z^*) = \{\theta \in \Theta : A(z^*)\theta \in -N_{\Omega}(z^*)\}$ (Theorem 9). For $\mathcal{IL}/\mathcal{ILCO}$, the analogous cone associated with the recovered solution’s active set is used.

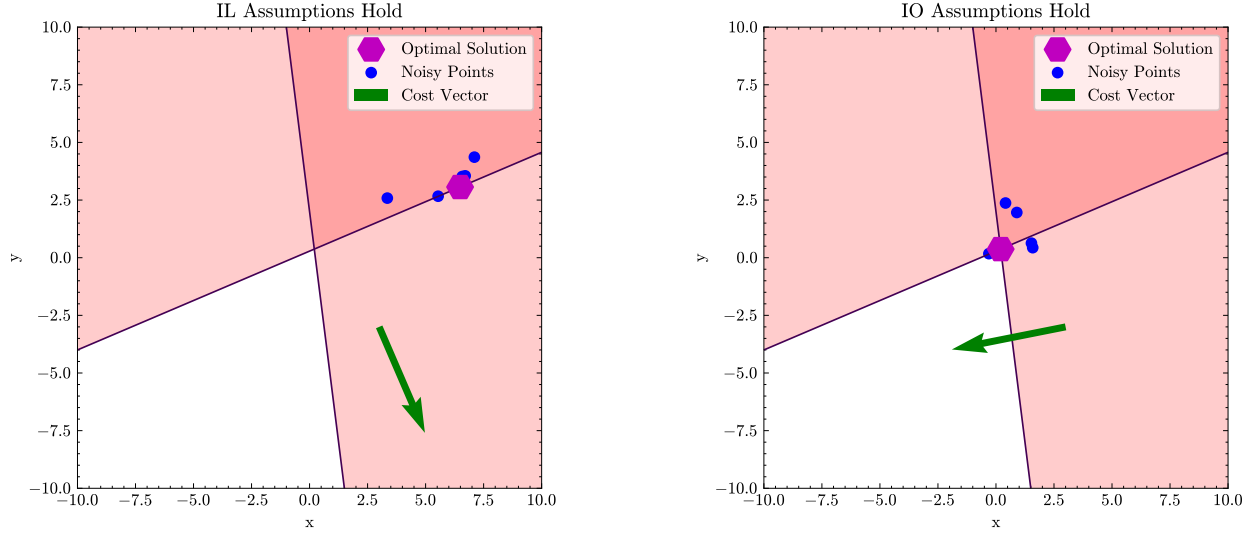


Figure 2 Data generation under the two experimental scenarios. (Left) IL Assumption Scenario: noise is added to a single true optimal solution x^* , consistent with Assumption 8. (Right) IO Assumption Scenario: noise is added to potentially different optimal solutions x_k^* for a single true parameter θ^* .

Computational Time. Average wall-clock time per instance.

For each configuration (noise level, knowledge level, binding parameter), 100 independent instances are generated and solved. All optimization models are implemented in Gurobi 11.0 via Python. The bilinear formulation (4) is solved using a decomposition approach for tractability, consistent with the discussion in Remark 2.

5.2. Results and Discussion

5.2.1. Solution Accuracy. Figure 3 presents the distribution of distances between learned solutions and the true optimal solution under the \mathcal{IL} Assumption Scenario for $n = 10$, across varying noise levels (columns) and true solution binding levels (rows). Five models are compared: \mathcal{IL} , \mathcal{GIL} with $r \in \{5, 10\}$, \mathcal{MGL} with $r \in \{5, 10\}$, and the classical benchmark \mathcal{ILO} .

Three findings emerge. First, the \mathcal{IL} framework models consistently produce solutions closer to the true x^* than the benchmark \mathcal{ILO} . This advantage is most pronounced when the true solution activates relatively few constraints (Binding = 1 and Binding = 5), where \mathcal{IL} achieves near-zero distances while \mathcal{ILO} produces solutions far from observations. Second, as r increases in \mathcal{GIL} and \mathcal{MGL} , the solution distance generally increases, quantitatively demonstrating the observation-constraint tradeoff formalized in Definition 2. This confirms the theoretical prediction: forcing more relevant constraints to bind (higher r) moves the solution further from the data centroid. Third, when the true solution itself binds many constraints (Binding = 10), all models converge in performance, as the constrained feasible set narrows substantially. The \mathcal{MGL} sequence (Theorem 10) exhibits

the expected monotone distance increase, consistent with the nested face structure (Theorem 11). Under the \mathcal{IO} Assumption Scenario, the qualitative patterns are similar, though absolute distances are generally larger for all models. The \mathcal{IL} models still provide solutions closer to the mean true solution compared to the extreme point typically returned by \mathcal{ILO} .

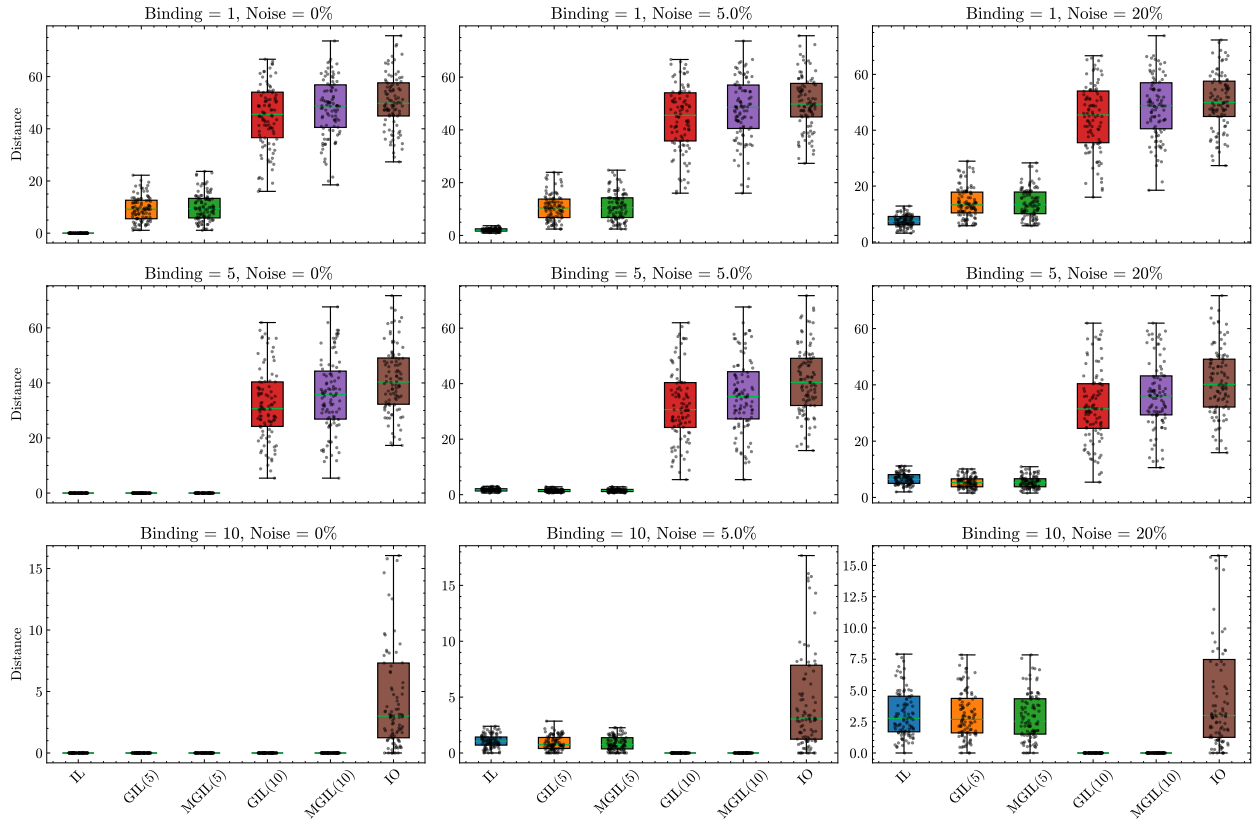


Figure 3 Solution distance comparison (ℓ_2 -norm to true solution) under the \mathcal{IL} Assumption Scenario ($n = 10$). Boxplots show distributions across 100 instances for varying noise levels (columns) and true solution binding levels (rows). Models include \mathcal{IL} , $\mathcal{GIL}(r)$, $\mathcal{MGIL}(r)$ with $r \in \{5, 10\}$, and the classical benchmark \mathcal{ILO} . The \mathcal{IL} framework models consistently yield smaller distances than \mathcal{ILO} . Distance increases with r , illustrating the observation-constraint tradeoff.

5.2.2. Parameter Recovery. Figures 5–7 present parameter recovery rates, i.e., the percentage of instances in which the true θ^* lies within the compatible cone $\Theta^*(z^*)$, as a function of the binding parameter r . We report results for \mathcal{GIL} and \mathcal{MGIL} , both with preferred constraints (using knowledge of a subset of truly binding constraints) and without preferred constraints (denoted $\mathcal{GIL_NK}$ and $\mathcal{MGIL_NK}$), alongside \mathcal{IL} and \mathcal{ILO} as flat baselines.

Several important patterns emerge. First, both \mathcal{GIL} and \mathcal{MGIL} achieve substantially higher recovery rates than \mathcal{IL} and \mathcal{ILO} as r increases. At low knowledge levels (Knowledge = 1),

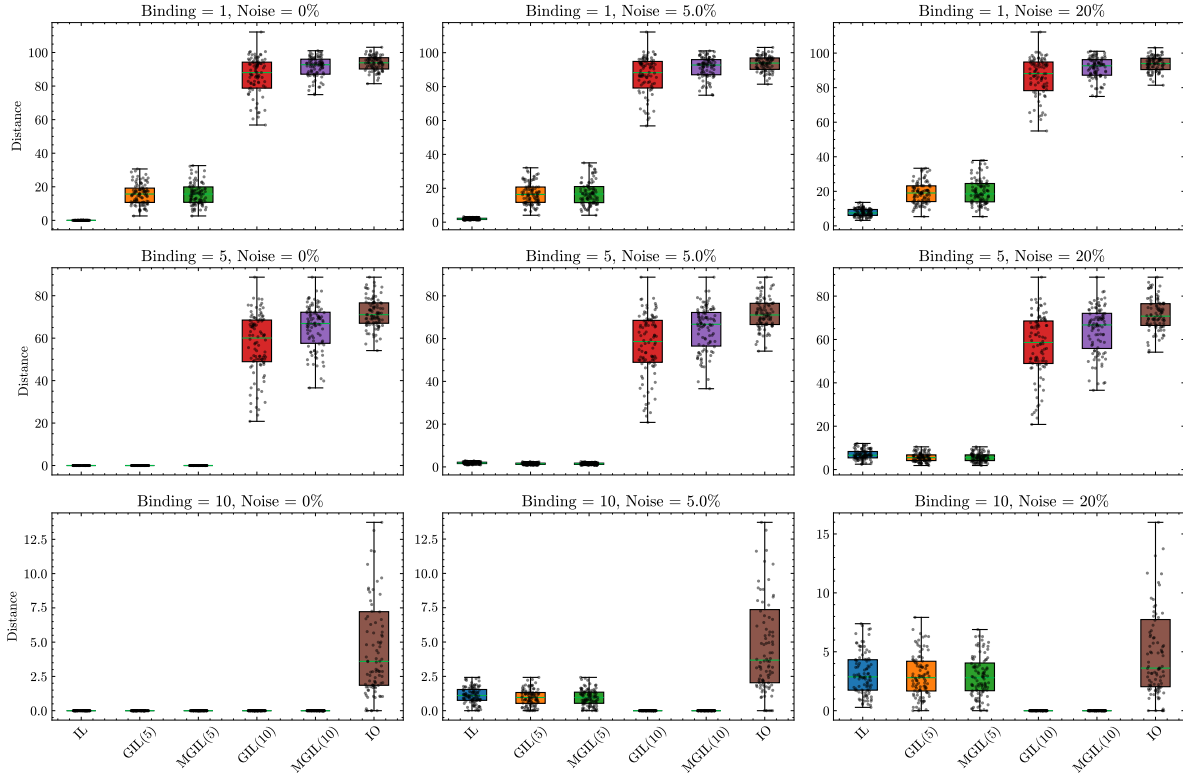


Figure 4 Solution distance comparison under the IO Assumption Scenario ($n = 10$). Structure and interpretation mirror Figure 3. IL framework models maintain their proximity advantage.

recovery rates approach 100% even at moderate r values, confirming that the cardinality parameter directly addresses the non-identifiability established in Theorems 1–2: by forcing more constraints to bind, the compatible cone $\Theta^*(z^*)$ is narrowed, increasing the likelihood that it contains the true parameter. Second, models with preferred constraints (GIL , $MGIL$) consistently outperform their no-knowledge counterparts (GIL_NK , $MGIL_NK$), validating the constraint hierarchy mechanism of Assumption 9. Third, performance degrades with increasing knowledge level (i.e., when the true solution binds many constraints), because the combinatorial challenge of identifying the correct active set grows. Even in these harder regimes, $MGIL$ with preferred constraints maintains a clear advantage.

Increasing noise degrades performance for all models, but the relative ranking persists. Notably, $MGIL$ with preferred constraints is the most robust to noise, consistent with its sequential constraint activation mechanism: inherited constraints from previous iterations provide stable structure even as the centroid \bar{x} shifts due to noise (Theorem 13).

Figure 8 compares all four model variants at a fixed noise level ($\sigma = 50\%$) across knowledge levels. When knowledge is low (Knowledge = 1), all models perform well. As the knowledge level increases

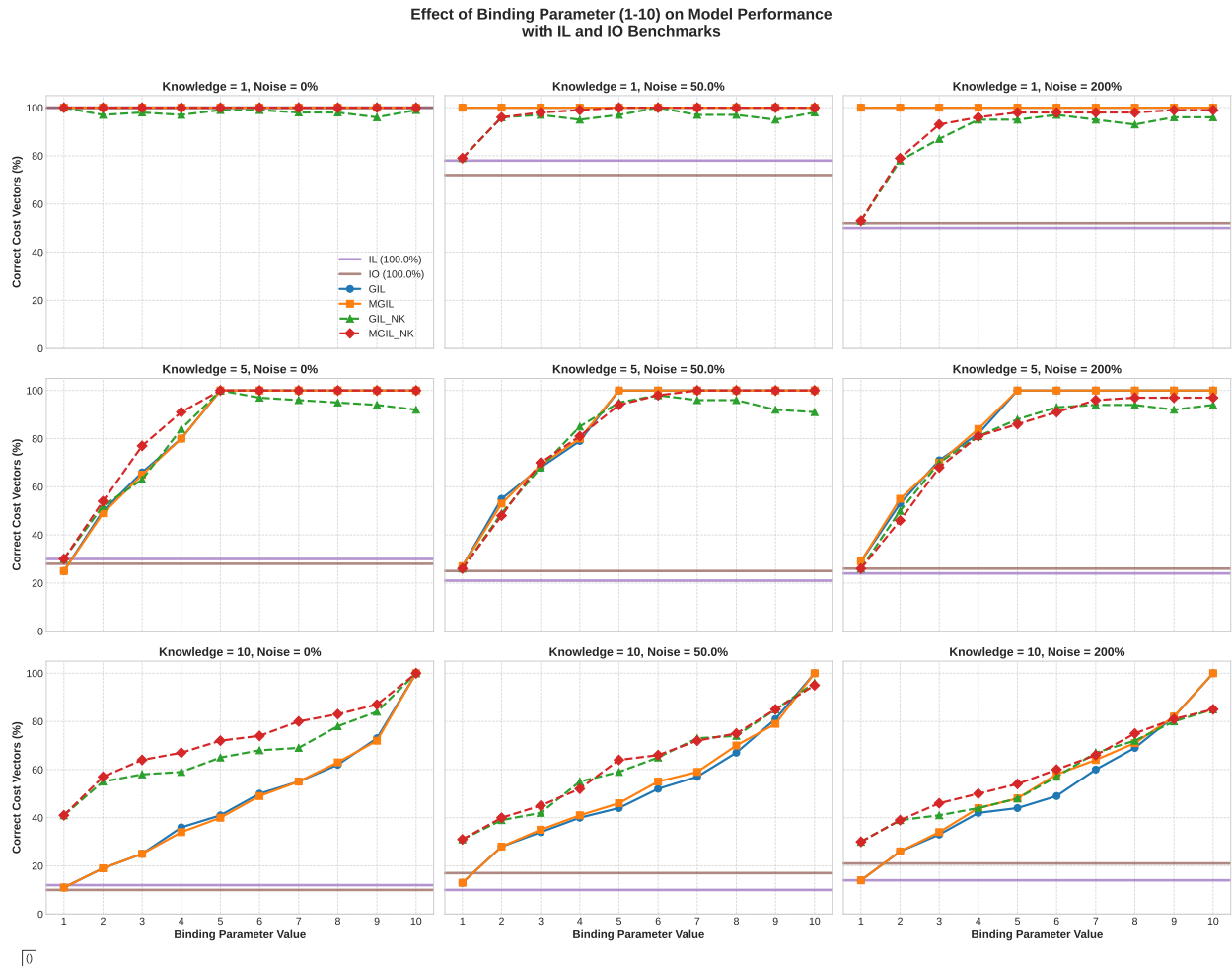


Figure 5 Parameter recovery rate as a function of the binding parameter r across knowledge levels (rows) and noise levels (columns). Flat lines represent IL and $ILCO$ baselines (independent of r). The goal-integrated models GIL and $MGIL$ (with and without preferred constraints, denoted “NK”) achieve monotonically increasing recovery rates with r , substantially outperforming the baselines. Preferred constraint knowledge provides consistent additional benefit.

(Knowledge = 5, 10), the gap between models with and without preferred constraints widens, and $MGIL$ with preferred constraints dominates uniformly.

5.2.3. Computational Efficiency. Table 3 reports average solution times across 100 instances for $n = 10$. $MGIL$ is consistently the fastest among the goal-integrated models, followed by GIL . The basic IL model is more expensive than the goal-integrated variants (which benefit from tighter feasible regions due to binding constraints), and the benchmark $ILCO$ (solved via LP decomposition) is significantly the slowest. This efficiency hierarchy is consistent with the complexity analysis in Theorem 4 and Proposition 11: the IL framework models have $O(n + m + p)$ variables independent of K , whereas $ILCO$ requires $O(Kn + Km)$ variables.

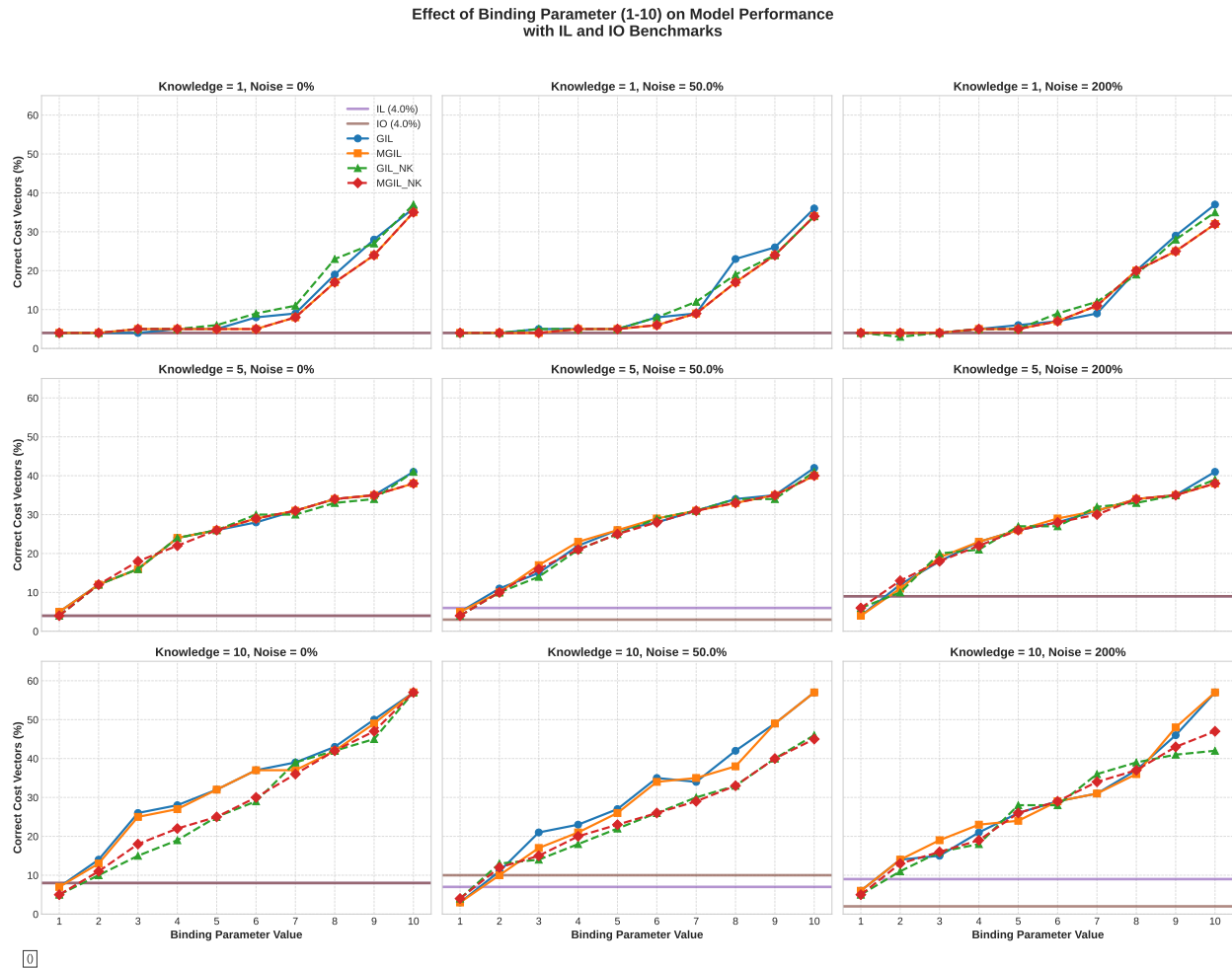


Figure 6 Parameter recovery rate under the IO Assumption Scenario. The $GIL/MGIL$ models maintain their advantage even under classical IO assumptions, demonstrating robustness to the data-generating mechanism.

The numerical experiments validate the theoretical properties established in Sections 3–4. The IL framework models, particularly GIL and $MGIL$, offer three advantages over classical $ILCO$: (i) superior solution proximity to the true optimal solution, (ii) substantially higher parameter recovery rates when structural knowledge is incorporated through the binding parameter r and preferred constraints \mathcal{P} , and (iii) significant computational speedups due to K -independence (Theorem 4). These advantages are robust across data generation scenarios, noise levels, and structural configurations, confirming that the goal-integrated approach provides a principled mechanism for navigating the observation-constraint tradeoff (Definition 2).

6. Application: Personalized Diet Recommendations via Inverse Learning

We demonstrate the practical value of the Inverse Learning framework through a healthcare application: generating dietary recommendations for patients with hypertension. In this domain,

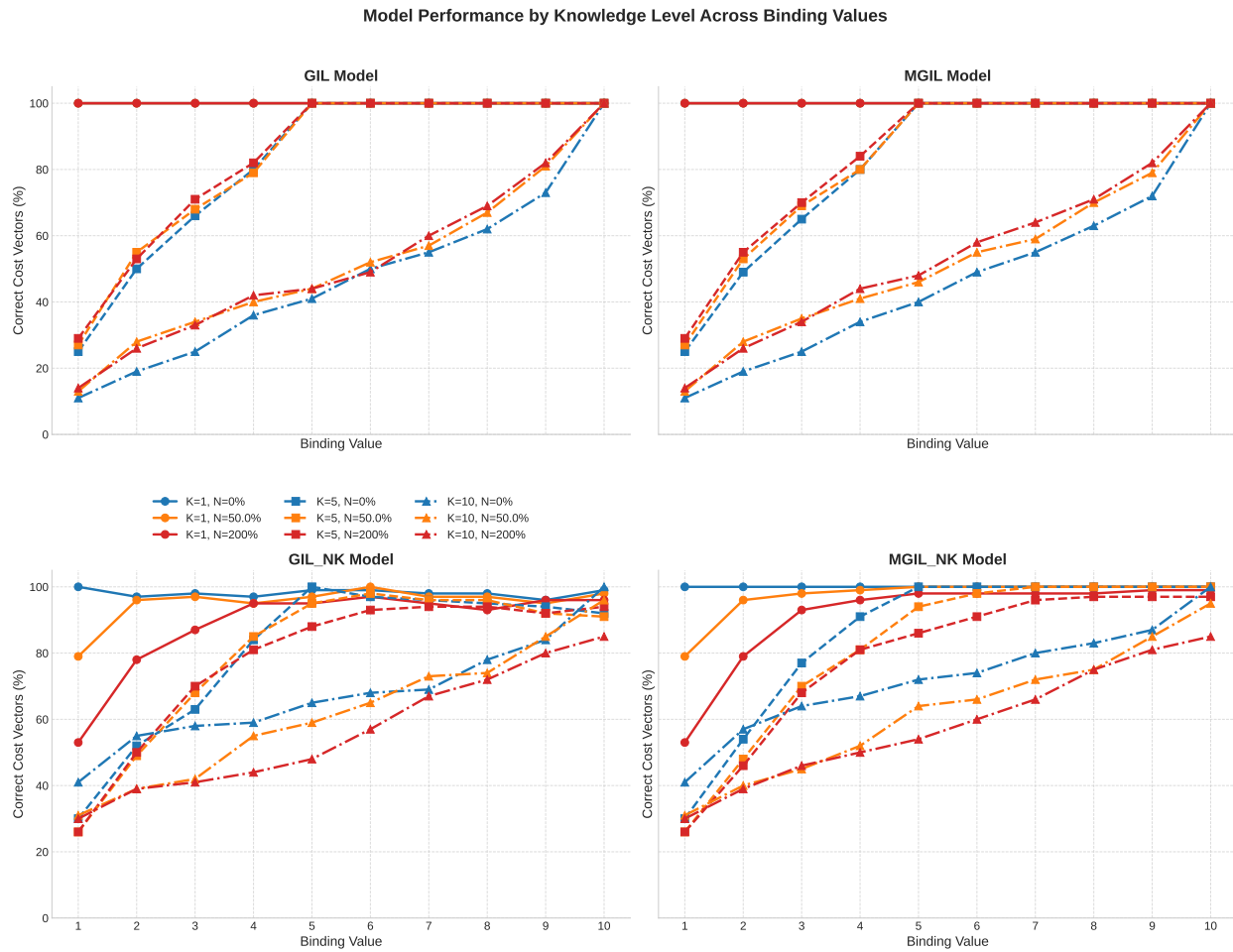


Figure 7 Disaggregated parameter recovery performance by model type. Each panel isolates one model variant, showing how recovery rates vary across knowledge levels (K) and noise levels (N). Models with preferred constraints (top row) exhibit higher recovery rates, especially at low binding values r , confirming the value of the constraint hierarchy (Assumption 9).

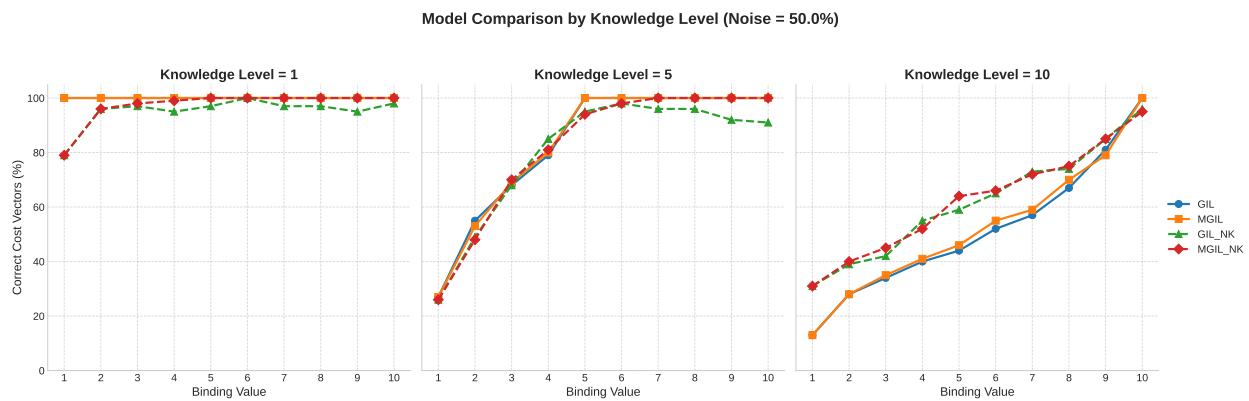


Figure 8 Model comparison by knowledge level at fixed noise ($\sigma = 50\%$). At low knowledge levels, all models perform comparably. At higher knowledge levels, the advantage of preferred constraints and sequential constraint activation ($MGIL$) becomes pronounced.

expert guidelines such as the Dietary Approaches to Stop Hypertension (DASH) diet define nutritional targets that patients should satisfy. However, strict adherence is often poor due to the gap between guidelines and eating habits. The \mathcal{IL} framework addresses this by treating observed dietary behavior as noisy observations of an individual’s latent optimal diet (Assumption 8), then navigating the tradeoff between preserving habitual patterns and satisfying nutritional constraints.

6.1. Data Sources and Feasible Set Construction

The application requires two inputs: observational data \mathcal{X} reflecting dietary behavior, and a feasible region Ω encoding expert nutritional guidelines.

Observational Data. We use the National Health and Nutrition Examination Survey (NHANES) dataset (CDC 2020), which contains detailed two-day, self-reported dietary intake records for 9,544 individuals. From this cohort, we identify 2,090 individuals who self-reported a hypertension diagnosis, yielding 4,024 daily intake observations. These observations constitute \mathcal{X} .

Feasible Region. The feasible region Ω is defined using linear constraints derived from the DASH diet (Sacks et al. 2001, Liese et al. 2009). Specifically, lower and upper bounds on 22 key nutrients (sodium, potassium, fats, carbohydrates, fiber, protein, etc.) are established based on DASH guidelines and tailored to demographic clusters defined by age and gender. These nutritional bounds form the relevant constraints \mathcal{R} (Assumption 9). Nutrient content per serving is obtained from the USDA FoodData Central database (USDA 2019); approximately 5,000 detailed food types are aggregated into 38 food groups (Electronic Companion Table EC.1), defining the constraint coefficient matrices. Box constraints (0–8 servings per food group per day) form the trivial constraints \mathcal{T} . Sample nutrient bounds and food group coefficients for one demographic group are shown in Table 4.

Focus Population. For detailed analysis, we focus on a subgroup of 230 female patients aged 51+ reporting both hypertension and pre-diabetes, yielding 460 daily observations. Descriptive statistics for this subgroup are presented in Table 5. A comparison with DASH bounds reveals substantial non-adherence: average sodium intake (3,413 mg) exceeds the DASH upper limit (2,300 mg), with over 70% of observations violating this constraint. This gap exemplifies the practical challenge addressed by the Goal-Integrated framework: bridging observed behavior and expert guidelines through the observation-constraint tradeoff.

6.2. Retrospective Diet Recommendations

We apply the \mathcal{IL} framework retrospectively to the NHANES data. Under Assumption 8, each patient’s observed intake is treated as a noisy measurement of their latent preferred diet, and the relevant constraints encode DASH nutritional targets.

We use the ℓ_1 -norm for the distance metric in the \mathcal{IL} objectives. To generate sufficient variability for multi-observation analysis, 20 noisy perturbations are generated around each of the 460 real observations, creating input sets for the models. The \mathcal{IL} model (8) is solved for each set, yielding a recommended diet z^* that represents the minimal adjustment from the observed pattern required to achieve forward optimality while satisfying DASH constraints. Figure 9 compares the distribution of recommended food group intakes against the original observations. The \mathcal{IL} recommendations maintain structural similarity to observed patterns while ensuring feasibility—a direct consequence of the centroid projection property (Proposition 7).

The \mathcal{MGLL} model (15) is then applied iteratively, starting from the \mathcal{IL} solution and sequentially binding additional DASH nutritional constraints (Algorithm 1). This generates a sequence of diets z_0, z_1, \dots, z_L corresponding to increasing values of active relevant constraints. Figure 10 displays the resulting nutrient distributions for different levels of constraint activation ($r = 1, 2, 3, 4$). As r increases, nutrient distributions tighten around DASH targets: sodium decreases toward the 2,300 mg upper limit, fiber increases toward the 25 g lower bound, and saturated fat decreases. This demonstrates the monotone distance sequence (Theorem 10) in practice: each step increases adherence to nutritional guidelines at the cost of greater deviation from observed behavior.

These results demonstrate how the \mathcal{GIL} framework empowers practitioners to select personalized diets across the tradeoff spectrum. A dietitian might start with the \mathcal{IL} solution (minimal change from habitual behavior) and progressively tighten adherence via \mathcal{MGLL} , assessing at each step whether the marginal cost $\Delta D_\ell = D_{\ell+1} - D_\ell$ (Corollary 4) in behavioral deviation is acceptable. The framework can be further customized by specifying preferred constraints \mathcal{P} (e.g., prioritizing sodium reduction) within the \mathcal{GIL} objective (13a).

6.3. Prospective Feasibility Study

To assess real-world applicability, we conducted a prospective feasibility study with a healthy volunteer seeking a low-carbohydrate, 2,000-kcal diet. The participant wore a continuous glucose monitor (CGM) for two weeks. Week 1 served as baseline (usual diet logged). During Week 2, recommendations generated by applying \mathcal{MGLL} (with $r = 3$, prioritizing sugar reduction) to the baseline data were provided. The participant retained full autonomy over food choices.

Post-recommendation CGM data (Figure 11, Table 6) indicated improved glycemic control: mean glucose decreased from 81.9 to 77.2 mg/dL, and the proportion of readings exceeding 100 mg/dL dropped from 6.6% to 0.4%. Nutritional analysis (Tables 7–8, Figure 13) confirmed substantial reductions in targeted nutrients (calories -14.8% , sugar -40.4%) while maintaining intake of others (fat, fiber), reflecting the personalized nature of the recommendations. Food group

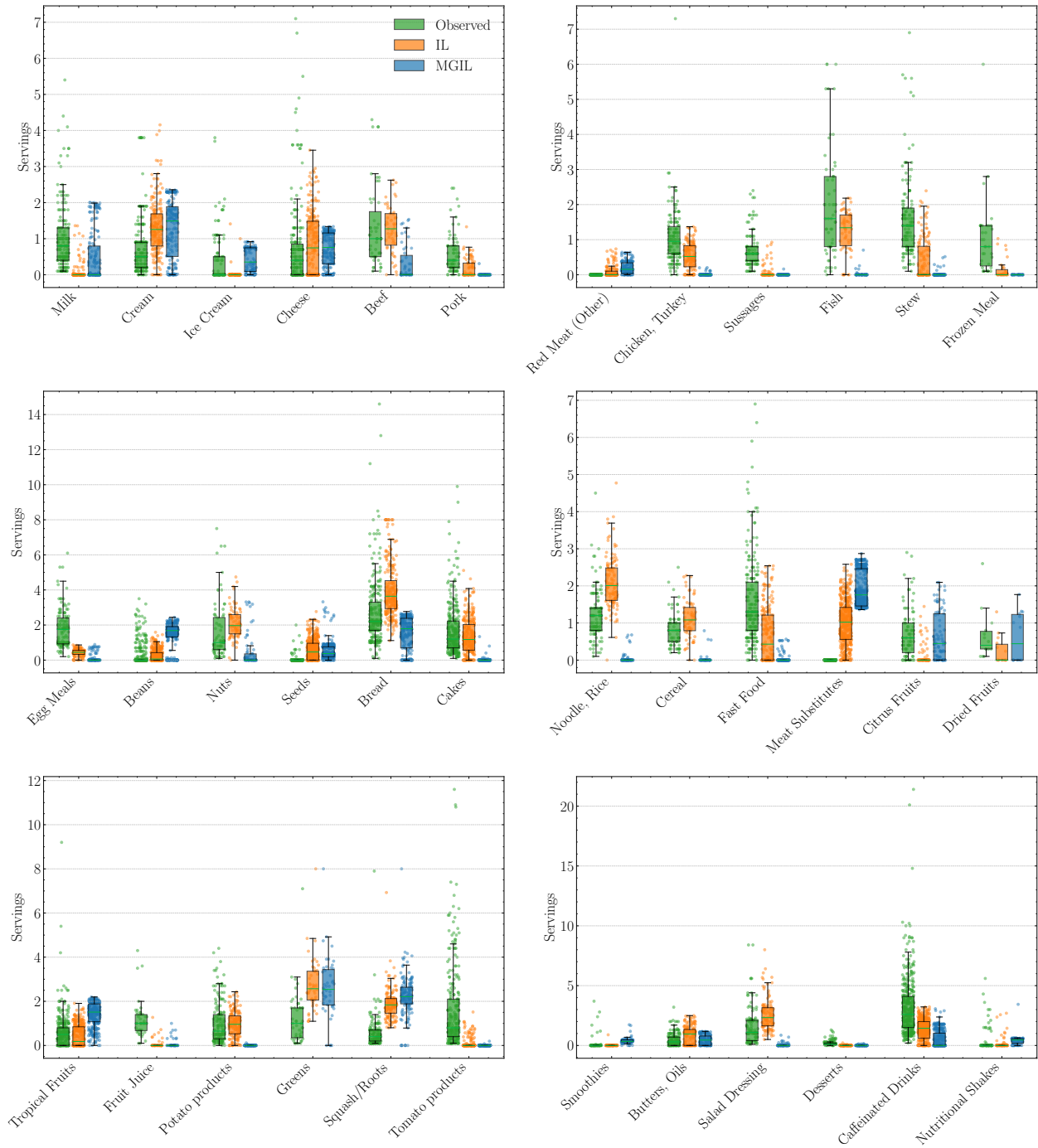


Figure 9 Comparison of observed daily food intakes (left, green; $N = 230$ patients) and recommended intakes from IL (8) (center, orange) and $MGIL$ (15) (right, blue) applied to perturbed observations. The IL model preserves the structure of observed patterns while ensuring feasibility. $MGIL$ with additional binding constraints produces further adjustments toward DASH guidelines.

analysis (Figure 12) indicated partial adherence, demonstrating both the model's ability to generate actionable recommendations and the practical complexities of dietary change.

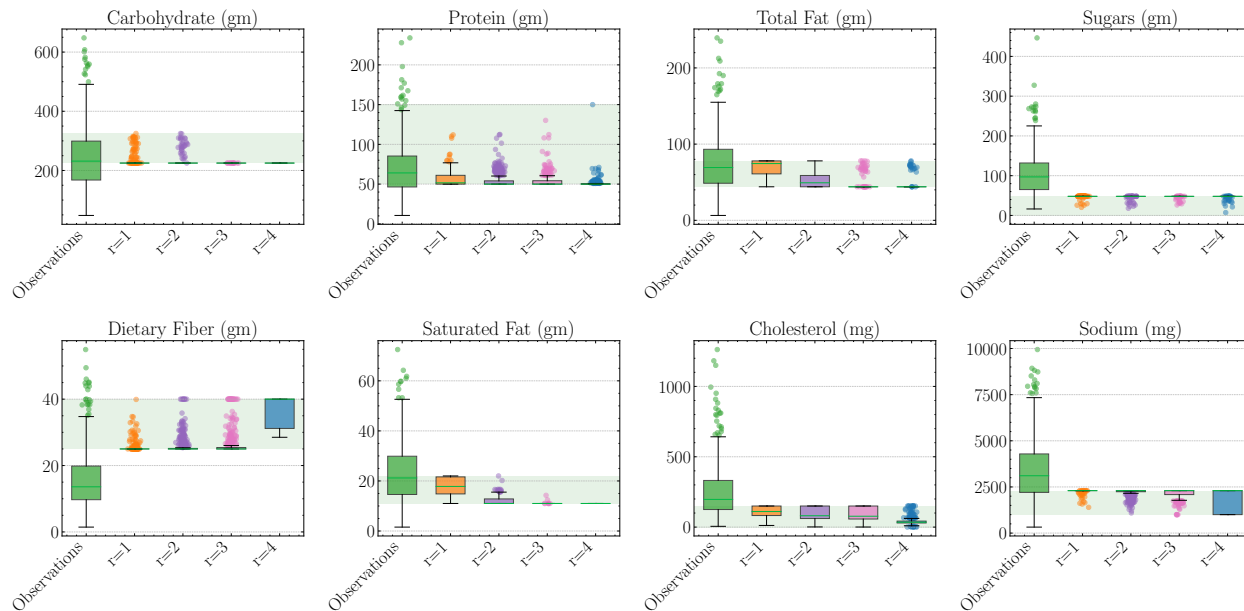


Figure 10 Distribution of key nutrient levels in diets recommended by iteratively applying $MGLL$ (15) for varying numbers of binding relevant constraints (r). Green shaded regions indicate DASH guideline bounds. As r increases, nutrient distributions progressively align with targets (e.g., sodium tightens toward 2,300 mg), illustrating the observation-constraint tradeoff (Definition 2).

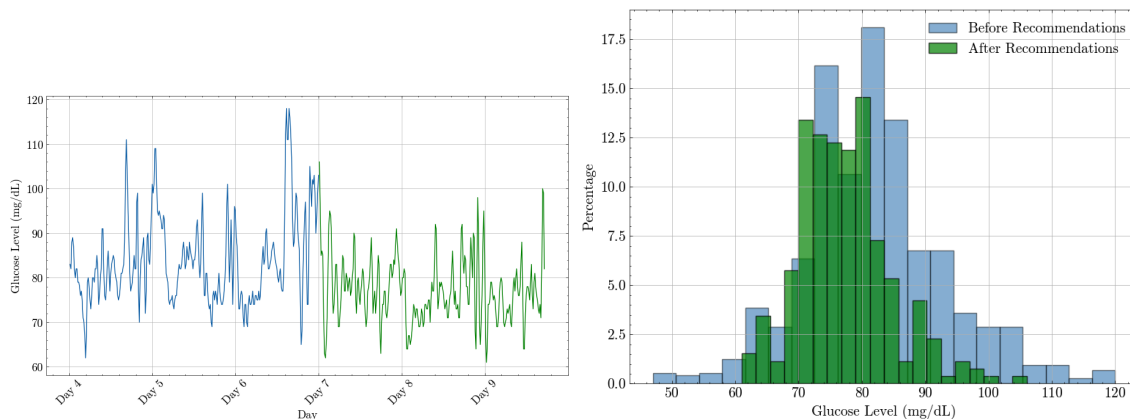


Figure 11 Continuous glucose monitoring (CGM) data before (blue) and after (green) implementing $MGLL$ -based dietary recommendations. Left: time series of glucose readings. Right: histogram of glucose levels showing a shift toward lower, more concentrated values post-recommendation.

This single-participant study has clear limitations (short duration, healthy volunteer, no control group) and should be interpreted as a proof-of-concept rather than a clinical trial. Nevertheless, the results provide preliminary evidence that the \mathcal{IL} framework can generate personalized, actionable dietary recommendations that lead to measurable physiological improvements while respecting individual eating patterns. The framework’s theoretical guarantees, namely consistency

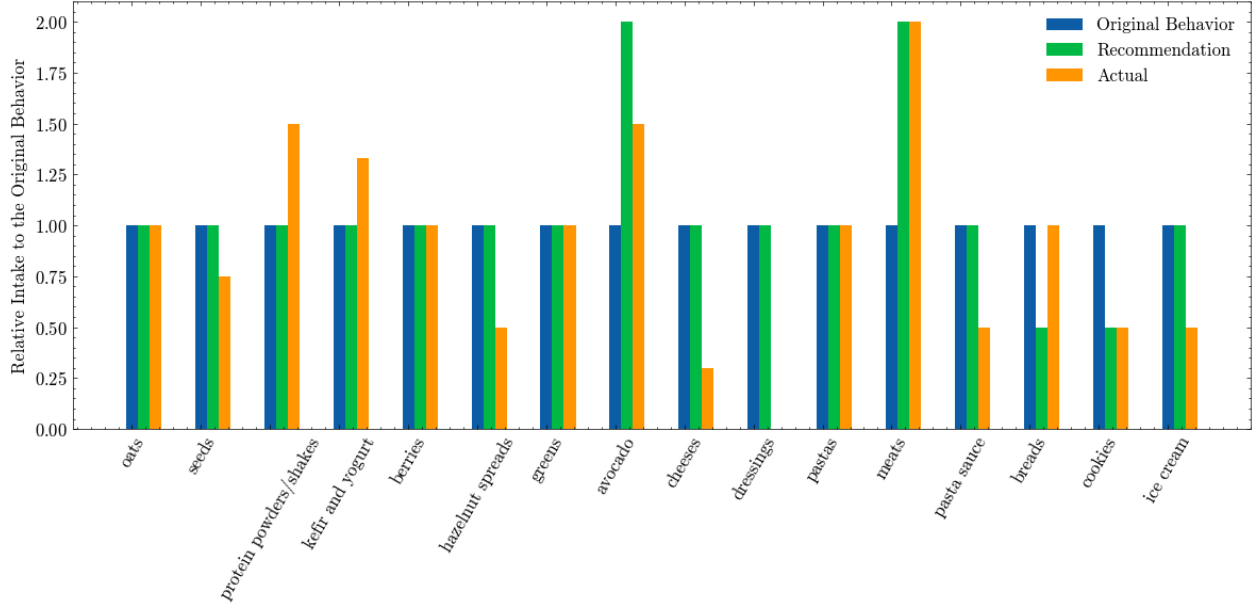


Figure 12 Comparison of original dietary behavior (blue), recommended adjustments from *MGIL* (green), and actual post-recommendation behavior (orange) across food groups. Values are normalized relative to original behavior (1.0). Partial adherence is visible: the participant increased avocado and meat intake as recommended, while decreasing cheeses and hazelnut spreads beyond the recommendation level.

(Theorem 13), monotone tradeoff navigation (Theorem 10), and full parameter set characterization (Theorem 9), provide a rigorous foundation for the dietary recommendations, distinguishing this approach from ad hoc clinical heuristics. The nested face structure (Theorem 11) ensures that as constraint adherence increases, all previously satisfied nutritional targets remain satisfied.

7. Conclusion

This paper develops a unified theoretical and computational framework for inverse optimization in parametric convex models. We show that parameter non-identifiability is structurally inherent in inverse convex optimization, establish conditions that separate identifiable from non-identifiable information, and introduce *Inverse Learning* (\mathcal{IL}) as a scalable alternative to classical formulations. In \mathcal{IL} (Section 3), the inferential target shifts from recovering the unknown parameter θ_0 to learning the latent optimal solution z_0 directly from data, mitigating non-identifiability while improving computational tractability. We further formalize the Observation-Constraint Tradeoff (Definition 2) via *Goal-Integrated Inverse Learning* (Section 4): *GIL* controls the number of binding relevant constraints through a cardinality parameter r , and *MGIL* provides sequential navigation with monotone distance guarantees (Theorem 10) and nested face containment (Theorem 11).

Numerical experiments (Section 5) support the theory: \mathcal{IL} recovers solutions closer to the true optimum than classical inverse linear optimization baselines while reducing runtimes by an order

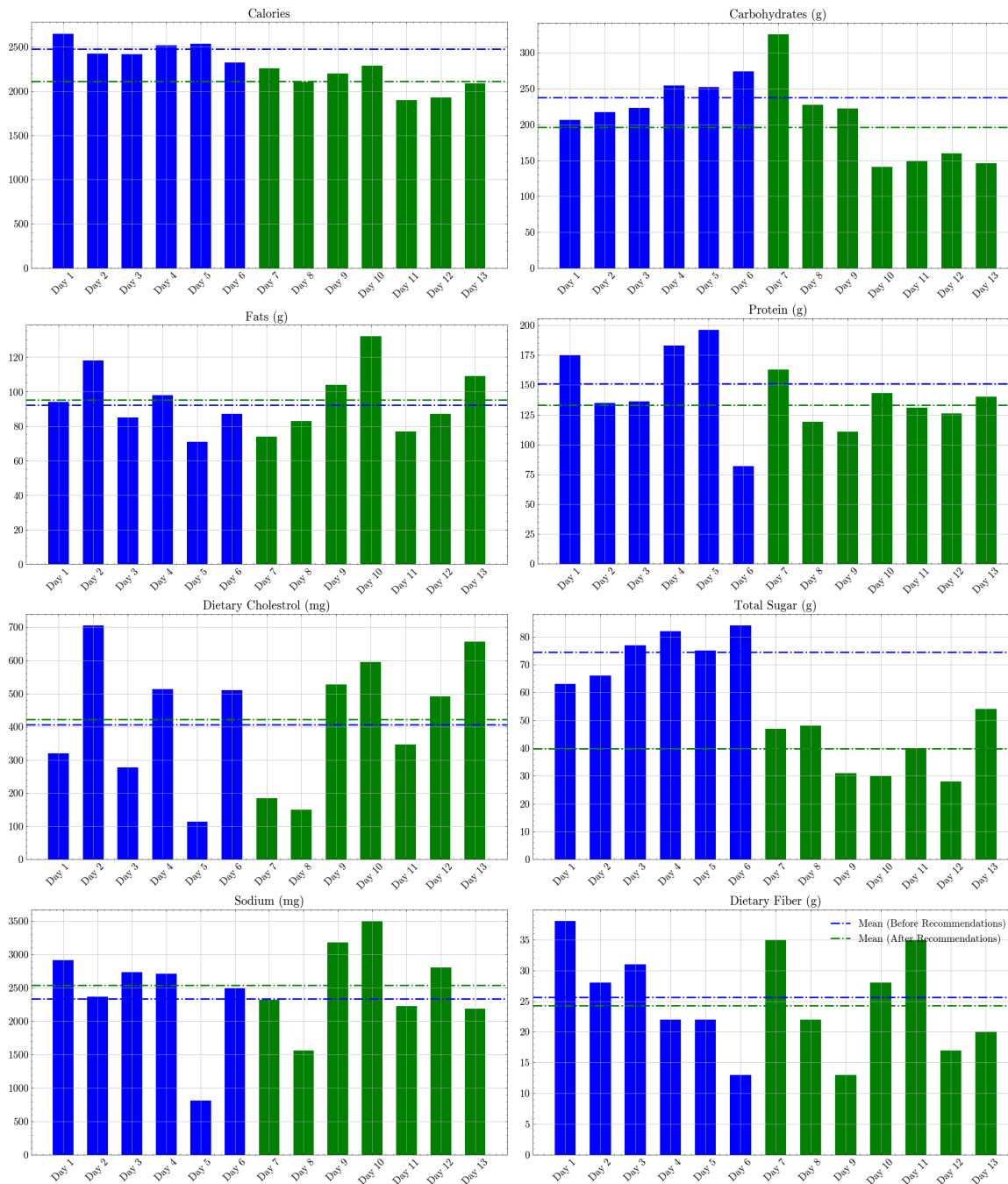


Figure 13 Daily nutrient intake before (blue) and after (green) implementation of *MGIL*-based dietary recommendations. Dashed lines indicate period means. Targeted nutrients (calories, carbohydrates, sugar) show clear reductions post-recommendation, while non-targeted nutrients (fat, fiber) remain relatively stable, demonstrating the personalized nature of the *MGIL* approach.

of magnitude, and goal-integrated variants improve parameter recovery when preferred constraint knowledge is available. A dietary case study (Section 6) illustrates how the framework can bridge

habitual behavior and DASH nutritional guidelines, with a prospective feasibility study providing preliminary evidence of improved glycemic control.

Several limitations remain. First, the current \mathcal{IL} framework assumes observations are noisy realizations of a single latent optimal solution (Assumption 8); this matches repeated decisions under stationary conditions but does not capture heterogeneous populations or time-varying preferences. When observations arise from multiple optima (e.g., across individuals or changing contexts), classical multi-observation formulations may be more appropriate, and the choice between \mathcal{IL} and \mathcal{ICO} should reflect the assumed data-generating process. Second, while \mathcal{IL} and its goal-integrated extensions remove dependence on the number of observations K , the current formulations remain nonconvex due to bilinearities and complementarity constraints and are handled via mixed-integer reformulations (linear case) or local/heuristic methods (general convex case); further research is needed to develop scalable decomposition and cutting-plane methods, particularly for very large instances where \mathcal{GIL} and \mathcal{MGIL} introduce m binary variables. Third, the dietary application is proof-of-concept: the prospective study involved a single healthy volunteer over a short duration without a control group, and further evaluation in larger randomized studies with target patient populations is needed to assess clinical efficacy.

Looking forward, several extensions would broaden applicability and strengthen statistical guarantees. The current work assumes a common latent optimum; extending \mathcal{IL} to contextual and heterogeneous settings, where objectives or constraints depend on covariates, would enable personalization while preserving computational advantages, but requires new modeling and algorithms that share information across contexts beyond naive partitioning (Besbes et al. 2023). The centroid’s streaming property suggests online and adaptive variants with regret guarantees and change-detection for shifts in the latent optimum, potentially leveraging the sequential structure of \mathcal{MGIL} for adaptive constraint-activation paths. For uncertainty quantification, $\Theta^*(z^*)$ is set-valued and not directly probabilistic; integrating conformal inverse optimization ideas could yield coverage-guaranteed uncertainty sets while retaining K -independent scalability (Lin and Others 2024). Finally, the current framework focuses on convex forward models; extending the non-identifiability analysis and goal-integrated mechanisms to nonlinear nonconvex and integer forward problems would expand relevance to combinatorial domains such as scheduling and routing, building on but going beyond existing inverse integer programming foundations (Schaefer 2009).

Code and Data Availability

All code used in the numerical experiments (Sections 5–6) is available at <https://anonymous.4open.science/r/Dietary-Behavior-Dataset-946C/README.md>, along with a README file describing the computational environment, data preparation steps, and instructions for

reproducing all reported results. The NHANES dietary intake data used in Section 6 are publicly available from the U.S. Centers for Disease Control and Prevention (CDC 2020). Nutrient composition data are publicly available from the USDA FoodData Central database (USDA 2019). The interactive decision-support tools described in Section EC.2 are accessible at <https://optimal-lab.com/nutrition-recommender/> and <https://optimal-lab.com/optimal-diet>. All optimization models were implemented using Gurobi 11.0 via Python; solver version and package dependencies are documented in the README.

References

- Ahuja RK, Orlin JB (2001) Inverse optimization. *Operations Research* 49(5):771–783.
- Ajayi T, Lee T, Schaefer AJ (2022) Objective selection for cancer treatment: an inverse optimization approach. *Operations Research* .
- Aswani A, Shen ZJ, Siddiq A (2018) Inverse optimization with noisy data. *Operations Research* 66(3):870–892.
- Bertsimas D, Gupta V, Paschalidis IC (2012) Inverse optimization: A new perspective on the black-litterman model. *Operations research* 60(6):1389–1403.
- Bertsimas D, Gupta V, Paschalidis IC (2015) Data-driven estimation in equilibrium using inverse optimization. *Mathematical Programming* 153(2):595–633.
- Besbes O, Fonseca Y, Lobel I (2023) Contextual inverse optimization: Offline and online learning. *Operations Research* .
- CDC (2020) Nhanes dietary data. URL <https://www.cdc.gov/nchs/nhanes/Search/DataPage.aspx?Component=Dietary>.
- Chan TC, Craig T, Lee T, Sharpe MB (2014) Generalized inverse multiobjective optimization with application to cancer therapy. *Operations Research* 62(3):680–695.
- Chan TC, Lee T, Terekhov D (2019) Inverse optimization: Closed-form solutions, geometry, and goodness of fit. *Management Science* 65(3):1115–1135.
- Chan TC, Mahmood R, Zhu IY (2024) Inverse optimization: Theory and applications. *Operations Research* 72(4):1427–1454.
- Chow JY, Recker WW (2012) Inverse optimization with endogenous arrival time constraints to calibrate the household activity pattern problem. *Transportation Research Part B: Methodological* 46(3):463–479.
- DASH (2018) Dash eating plan. URL <https://www.nhlbi.nih.gov/health-topics/dash-eating-plan>.
- Dong C, Chen Y, Zeng B (2018) Generalized inverse optimization through online learning. *Advances in Neural Information Processing Systems*, 86–95.
- Elmachtoub AN, Grigas P (2022) Smart “predict, then optimize”. *Management Science* 68(1):9–26, URL <http://dx.doi.org/10.1287/mnsc.2020.3922>.
- Esfahani PM, Shafieezadeh-Abadeh S, Hanasusanto GA, Kuhn D (2018) Data-driven inverse optimization with imperfect information. *Mathematical Programming* 167(1):191–234.

- Heuberger C (2004) Inverse combinatorial optimization: A survey on problems, methods, and results. *Journal of combinatorial optimization* 8(3):329–361.
- Iyengar G, Kang W (2005) Inverse conic programming with applications. *Operations Research Letters* 33(3):319–330.
- Keshavarz A, Wang Y, Boyd S (2011) Imputing a convex objective function. *2011 IEEE International Symposium on Intelligent Control*, 613–619 (IEEE).
- Liese AD, Nichols M, Sun X, D’Agostino RB, Haffner SM (2009) Adherence to the dash diet is inversely associated with incidence of type 2 diabetes: the insulin resistance atherosclerosis study. *Diabetes care* 32(8):1434–1436.
- Lin Y, Others (2024) Conformal inverse optimization. *arXiv preprint* .
- Ratliff LJ, Jin M, Konstantakopoulos IC, Spanos C, Sastry SS (2014) Social game for building energy efficiency: Incentive design. *2014 52nd Annual Allerton Conference on Communication, Control, and Computing (Allerton)*, 1011–1018 (IEEE).
- Rockafellar RT, Wets RJB (2009) *Variational Analysis* (Springer Science & Business Media).
- Sacks FM, Svetkey LP, Vollmer WM, Appel LJ, Bray GA, Harsha D, Obarzanek E, Conlin PR, Miller ER, Simons-Morton DG, et al. (2001) Effects on blood pressure of reduced dietary sodium and the dietary approaches to stop hypertension (dash) diet. *New England journal of medicine* 344(1):3–10.
- Saez-Gallego J, Morales JM, Madsen H (2017) Short-term forecasting of price-responsive loads using inverse optimization. *IEEE Transactions on Smart Grid* 9(5):4805–4814.
- Schaefer AJ (2009) Inverse integer programming. *Optimization Letters* 3(4):483–489.
- Shahmoradi Z, Lee T (2022) Quantile inverse optimization: Improving stability in inverse linear programming. *Operations research* 70(4):2538–2562.
- USDA (2019) Fooddata central. URL fdc.nal.usda.gov.
- Utz S, Wimmer M, Hirschberger M, Steuer RE (2014) Tri-criterion inverse portfolio optimization with application to socially responsible mutual funds. *European Journal of Operational Research* 234(2):491–498.
- Zattoni Scroccaro P, Atasoy B, Mohajerin Esfahani P (2025) Learning in inverse optimization: Incenter cost, augmented suboptimality loss, and algorithms. *Operations Research* 73(5):2661–2679, URL <http://dx.doi.org/10.1287/opre.2023.0254>.

8. Tables

Table 1 Complexity comparison between classical inverse optimization and Inverse Learning.

	\mathcal{ICO}	\mathcal{IL}
Variables	$O(Kn + Km + p)$	$O(n + m + p)$
Constraints	$O(Kn + Km)$	$O(n + m)$
Dependence on K	Linear	None

Table 2 Comparison of identifiability requirements for classical \mathcal{ICO} parameter recovery vs. \mathcal{IL} solution recovery.

Requirement	Classical \mathcal{ICO}	\mathbf{IL}
Target of identification	Parameter θ_0	Solution z_0
Normal cone dimension	Must be 1	Any dimension
Excitation condition	$S \succ 0$ required	Not required
Local convexity of \mathcal{Z}^*	Not explicitly required	Required locally
Achieves unique θ	Yes (under conditions)	Returns set Θ^*
Achieves unique z	Not necessarily	Yes

Table 3 Average solution times (seconds per 100 instances, $n = 10$) across models and data generation scenarios. $GIL/MGIL$ times reflect the maximum observed across tested r values. The classical \mathcal{ICO} formulation was solved via LP decomposition due to bilinear terms.

Data Scenario	\mathcal{ICO}^*	\mathcal{IL}	GIL	$MGIL$
\mathcal{IL} Assumptions	46.85	14.75	6.23	3.58
\mathcal{ICO} Assumptions	47.40	15.48	4.67	3.21

*Classical \mathcal{ICO} (4) solved via decomposition into a sequence of LPs. Otherwise \mathcal{ICO} exceeded 10000s in many instances.

Table 4 DASH nutrient bounds (relevant constraints) for women, age 51+, and sample nutrient coefficients per serving.

Nutrient	DASH Bounds		Nutrient Per Serving (Sample Foods)			
	Lower	Upper	Milk (244g)	Stew (140g)	Bread (25g)	Trop. Fruits (182g)
Carbs (g)	225*	325	18.8	21.3	12.3	27.8
Protein (g)	50	150*	7.2	16.8	2.5	1.4
Total Fat (g)	45*	80	6.3	14.3	1.5	1.9
Total Sugars (g)	0*	100	18.0	4.5	1.7	19.0
Fiber (g)	25	40*	0.2	1.5	0.9	4.1
Sat. Fat (g)	10*	22	3.3	4.6	0.4	0.31
Cholesterol (mg)	0*	150	14.0	53.9	1.2	0.0
Sodium (mg)	1000*	2300	108.3	639.4	119.0	10.7

* Indicates the bound designated as relevant in this setup.

Table 5 Descriptive statistics of observed daily nutrient intake for the focus subgroup (Women, 51+, Hypertension and Pre-diabetes, $N = 230$, 460 observations).

Nutrient	Mean	Std Dev	Min	25%	50%	75%	Max
Energy (kcal)	1,889.8	787.1	400.5	1,329.3	1,780.9	2,323.6	4,969.5
Carbohydrates (g)	242.5	105.3	48.1	167.7	231.6	299.2	647.9
Protein (g)	69.6	34.1	10.6	46.4	64.1	85.3	233.9
Total Fat (g)	74.6	36.8	6.4	48.7	69.3	93.2	239.4
Sugars (g)	104.9	54.8	16.3	65.0	96.9	131.9	446.6
Fiber (g)	15.6	8.8	1.5	9.7	13.6	19.8	54.9
Sat. Fat (g)	23.0	11.5	1.6	14.6	21.2	29.9	72.5
Cholesterol (mg)	250.2	192.9	5.5	124.8	196.9	331.7	1,262.0
Sodium (mg)	3,413.4	1,643.2	324.7	2,205.5	3,106.6	4,288.4	9,942.8

Table 6 Summary statistics of CGM data before and after dietary recommendations.

Statistic	Before	After
Mean (mg/dL)	81.90	77.17
Median (mg/dL)	81.00	76.00
Minimum (mg/dL)	47.00	61.00
Maximum (mg/dL)	120.00	106.00
Standard Deviation (mg/dL)	11.30	7.29
% Readings >100 mg/dL	6.63%	0.38%
% Readings 60–100 mg/dL	91.30%	99.62%

Table 7 Daily nutritional intake over the two-week study period.

Date	Calories	Carbs (g)	Fat (g)	Protein (g)	Cholest. (mg)	Sodium (mg)	Sugar (g)	Fiber (g)
Day 1	2,646	206	94	175	320	2,916	63	38
Day 2	2,420	217	118	135	705	2,366	66	28
Day 3	2,416	223	85	136	278	2,732	77	31
Day 4	2,515	254	98	183	513	2,709	82	22
Day 5	2,535	252	71	196	114	813	75	22
Day 6	2,324	274	87	82	511	2,492	84	13
Day 7	2,256	325	74	163	184	2,318	47	35
Day 8	2,102	227	83	119	150	1,560	48	22
Day 9	2,200	222	104	111	528	3,181	31	13
Day 10	2,289	141	132	143	595	3,497	30	28
Day 11	1,898	149	77	131	347	2,223	40	35
Day 12	1,930	160	87	126	491	2,805	28	17
Day 13	2,085	146	109	140	656	2,184	54	20

Table 8 Average daily nutrient intake before and after recommendations.

Nutrient	Before	After
Calories	2,445	2,084
Carbohydrates (g)	250	174
Fat (g)	90	98
Protein (g)	153	132
Sugar (g)	71	40
Fiber (g)	27	24

Electronic Companion

EC.1. Proof of Statements

Proof of Proposition 1 Each normal cone $N_\Omega(z^k) = \text{cone}\{a_i : i \in I(z^k)\}$ is a polyhedral cone by definition. The intersection of finitely many polyhedral cones is itself a polyhedral cone, establishing that \mathcal{C} is polyhedral.

For (i): If $i \in I_\cap$, then $i \in I(z^k)$ for all k , so $a_i \in N_\Omega(z^k)$ for all k , hence $a_i \in \mathcal{C}$. Since \mathcal{C} is a cone, $\text{cone}\{a_i : i \in I_\cap\} \subseteq \mathcal{C}$. Part (ii) follows directly from (i), and (iii) holds because a polyhedral cone has dimension 1 if and only if it is a single ray (a half-line from the origin). \square

Proof of Proposition 2 For (i): By Proposition 1(i), $\text{cone}\{a_i : i \in I_\cap\} \subseteq \mathcal{C}$. If $|I_\cap| \geq 2$ with $a_{i_1}, a_{i_2} \in \{a_i : i \in I_\cap\}$ not collinear, then a_{i_1} and a_{i_2} generate distinct rays in \mathcal{C} : neither is a positive scalar multiple of the other.

For (ii): With $K = 1$, $\mathcal{C} = N_\Omega(z^1) = \text{cone}\{a_i : i \in I(z^1)\}$. If $|I(z^1)| \geq 2$ with non-collinear generators, the cone has dimension at least 2, hence contains multiple rays.

For (iii): If $I(z^1) \subseteq I(z^k)$ for all k , then $N_\Omega(z^k) \supseteq N_\Omega(z^1)$ for all k (a larger active set generates a larger normal cone). Thus $\mathcal{C} = \bigcap_k N_\Omega(z^k) \supseteq N_\Omega(z^1)$, and the result follows from (ii).

For the converse: \mathcal{C} being a single ray means $\dim(\mathcal{C}) = 1$, which requires the constraints across all observations to collectively leave exactly one feasible objective direction. \square

Proof of Theorem 1 By Proposition 2, the stated conditions guarantee that \mathcal{C} contains at least two distinct rays, generated by linearly independent vectors $v^{(1)}, v^{(2)} \in \mathcal{C}$ with $v^{(1)}, v^{(2)} \neq 0$ and $v^{(2)} \neq \alpha v^{(1)}$ for any $\alpha > 0$.

Case 1: Euclidean normalization $\Theta = \{\theta : \|\theta\|_2 = 1\}$. Define $\theta^{(1)} = v^{(1)}/\|v^{(1)}\|_2$ and $\theta^{(2)} = v^{(2)}/\|v^{(2)}\|_2$. Since $v^{(1)}$ and $v^{(2)}$ generate distinct rays, $\theta^{(1)} \neq \theta^{(2)}$. Both lie in \mathcal{C} (cones are closed under positive scaling) and satisfy the normalization.

Case 2: Simplex normalization $\Theta = \{\theta : \mathbf{1}^\top \theta = 1, \theta \geq 0\}$. Since \mathcal{ICO} is assumed feasible, there exists at least one $\bar{\theta} \in \mathcal{C} \cap \Theta$; in particular $\bar{\theta} \geq 0$, $\bar{\theta} \neq 0$, so $\mathcal{C} \cap \mathbb{R}_+^n \neq \{0\}$.

We claim $\mathcal{C} \cap \Theta$ contains at least two distinct points. To see this, note that $\mathcal{C} \cap \mathbb{R}_+^n$ is a polyhedral cone. If $\dim(\mathcal{C} \cap \mathbb{R}_+^n) \geq 2$, then its intersection with the hyperplane $\{\theta : \mathbf{1}^\top \theta = 1\}$ is a polytope of dimension at least 1, hence it contains infinitely many points. It remains to show $\dim(\mathcal{C} \cap \mathbb{R}_+^n) \geq 2$.

Suppose for contradiction that $\dim(\mathcal{C} \cap \mathbb{R}_+^n) \leq 1$. Since \mathcal{C} has dimension at least 2 (by Proposition 2), any two-dimensional face of \mathcal{C} would need to lie entirely outside \mathbb{R}_+^n except along at most a single ray. However, under Assumption 3 (which restricts $\theta \in \mathbb{R}_+^n$), every feasible parameter of \mathcal{ICO} must lie in $\mathcal{C} \cap \mathbb{R}_+^n$. The existence of $\bar{\theta} \in \mathcal{C} \cap \mathbb{R}_+^n$ with $\bar{\theta} \neq 0$ combined with $\dim(\mathcal{C}) \geq 2$ and the fact that \mathcal{C} is generated by nonnegative combinations of constraint normals a_i (which, in

polyhedral inverse optimization, are the rows of A) ensures that \mathcal{C} possesses at least two linearly independent generators in \mathbb{R}_+^n , yielding $\dim(\mathcal{C} \cap \mathbb{R}_+^n) \geq 2$. (More precisely, $\mathcal{C} \subseteq \text{cone}\{a_i : i \in I_\cap\}$ by Proposition 1(i), and under the conditions of Proposition 2, at least two non-collinear a_i generate rays in \mathcal{C} . The nonnegativity of these generators depends on the problem data; if $a_{i_1}, a_{i_2} \in \mathbb{R}_+^n$, the conclusion follows immediately.)

Feasibility for ICCO: Each $\theta^{(i)} \in \mathcal{C}$ satisfies $\theta^{(i)} \in N_\Omega(z^k)$ for all k . This means there exist $\lambda^k \geq 0$ supported on $I(z^k)$ such that $\theta^{(i)} = \sum_{j \in I(z^k)} \lambda_j^k a_j$. Combined with primal feasibility $z^k \in \Omega$ and complementary slackness (automatic since λ^k is supported on the active set $I(z^k)$), z^k is optimal for $\min\{(\theta^{(i)})^\top x : x \in \Omega\}$. Since both $\theta^{(1)}$ and $\theta^{(2)}$ rationalize all observations as optimal, both are feasible for ICCO. \square

Proof of Corollary 1 In the linear case, the relaxed stationarity constraint in $\mathcal{R}\text{-ICCO}$ reads $\|\theta - A^\top \lambda^k\|_2 \leq \epsilon$ for $k = 1, \dots, K$, where $\lambda^k \geq 0$.

Let $v^{(1)}, v^{(2)} \in \mathcal{C}$ be distinct ray generators (existence guaranteed by Proposition 2). For each $v^{(i)}$ and each k , since $v^{(i)} \in N_\Omega(z^k) = \text{cone}\{a_j : j \in I(z^k)\}$, there exist nonnegative coefficients $\{\mu_j^{k,(i)}\}_{j \in I(z^k)}$ such that $v^{(i)} = \sum_{j \in I(z^k)} \mu_j^{k,(i)} a_j$. Define $\lambda^{k,(i)} \in \mathbb{R}^m$ by $\lambda_j^{k,(i)} = \mu_j^{k,(i)}$ for $j \in I(z^k)$ and $\lambda_j^{k,(i)} = 0$ otherwise. Then $A^\top \lambda^{k,(i)} = v^{(i)}$.

For the normalized parameter $\theta^{(i)} = v^{(i)} / \|v^{(i)}\|_2 \in \Theta$, set $\tilde{\lambda}^{k,(i)} = \lambda^{k,(i)} / \|v^{(i)}\|_2$. Then $A^\top \tilde{\lambda}^{k,(i)} = \theta^{(i)}$, yielding zero stationarity residual: $\|\theta^{(i)} - A^\top \tilde{\lambda}^{k,(i)}\|_2 = 0 \leq \epsilon$.

Since this construction applies to any ray generator in \mathcal{C} , each corresponding normalized $\theta^{(i)}$ is feasible for $\mathcal{R}\text{-ICCO}$ with zero stationarity residual. The existence of multiple distinct rays in \mathcal{C} therefore implies multiple feasible θ in $\mathcal{R}\text{-ICCO}$ for any $\epsilon \geq 0$. Moreover, the ϵ -relaxation only enlarges the feasible set beyond $\mathcal{C} \cap \Theta$, so any additional ambiguity compounds the underlying non-identifiability rather than resolving it. \square

Proof of Proposition 3 For each k , the constraint $A(z^k)\theta \in -N_\Omega(z^k)$ defines the preimage of the polyhedral cone $-N_\Omega(z^k)$ under the linear map $\theta \mapsto A(z^k)\theta$. Under Assumption 2, $N_\Omega(z^k) = \text{cone}\{\nabla g_i(z^k) : i \in I(z^k)\}$ is polyhedral. The preimage of a polyhedral cone under a linear map is a polyhedral cone, and the intersection of finitely many polyhedral cones is polyhedral. \square

Proof of Proposition 4 For (i): If $\theta_0 \in \bigcap_k \ker(A(z^k))$ with $\theta_0 \neq 0$, then $A(z^k)\theta_0 = 0 \in -N_\Omega(z^k)$ for all k (since every cone contains the origin). Thus $\theta_0 \in \mathcal{S}$. For any $\bar{\theta} \in \mathcal{S}$, we have $\bar{\theta} + \alpha\theta_0 \in \mathcal{S}$ for all $\alpha \in \mathbb{R}$, since $A(z^k)(\bar{\theta} + \alpha\theta_0) = A(z^k)\bar{\theta} \in -N_\Omega(z^k)$. If $\bar{\theta}$ is not parallel to θ_0 , then $\bar{\theta}$ and θ_0 generate two non-collinear rays in \mathcal{S} .

For (ii): Let $A := A(z^{k_0})$. Since A has full column rank, the map $\theta \mapsto A\theta$ is injective, establishing a linear bijection between \mathbb{R}^p and $\text{range}(A)$. The constraint from observation k_0 requires $A\theta \in -N_\Omega(z^{k_0})$, i.e.,

$$\theta \in A^{-1}(-N_\Omega(z^{k_0})) = \{\theta \in \mathbb{R}^p : A\theta \in -N_\Omega(z^{k_0})\}.$$

Because A is injective, the preimage cone $A^{-1}(-N_{\Omega}(z^{k_0}))$ is isomorphic (via A) to $\text{range}(A) \cap (-N_{\Omega}(z^{k_0}))$. In particular,

$$\dim(A^{-1}(-N_{\Omega}(z^{k_0}))) = \dim(\text{range}(A) \cap N_{\Omega}(z^{k_0})) \geq 2$$

by hypothesis. A polyhedral cone of dimension ≥ 2 contains at least two non-collinear rays, say $v^{(1)}, v^{(2)}$.

Since $\mathcal{S} \subseteq A^{-1}(-N_{\Omega}(z^{k_0}))$, two non-collinear rays in the preimage are elements of \mathcal{S} only if they also satisfy the constraints from all other observations. For $K = 1$ the conclusion follows immediately. For $K > 1$, the conclusion holds provided the constraints from observations $k \neq k_0$ do not reduce $\dim(\mathcal{S})$ below 2. This is guaranteed, for instance, when $I(z^{k_0}) \subseteq I(z^k)$ for all k (so that the k_0 -constraint is the most restrictive), paralleling Proposition 2

For (iii): If S is singular, there exists $\Delta\theta \neq 0$ with $S\Delta\theta = 0$. By definition of S , this implies $\|P_k A(z^k)\Delta\theta\|_2^2 = 0$ for each k , so $A(z^k)\Delta\theta \in \text{span}\{n^k\}$ for all k (under one-dimensional normal cones $N_{\Omega}(z^k) = \text{cone}\{n^k\}$). Writing $A(z^k)\Delta\theta = \beta_k n^k$, consider any $\bar{\theta} \in \mathcal{S}$ with $A(z^k)\bar{\theta} = -\alpha_k n^k$, $\alpha_k \geq 0$. Then for sufficiently small $t > 0$,

$$A(z^k)(\bar{\theta} + t\Delta\theta) = -(\alpha_k - t\beta_k)n^k,$$

and $\alpha_k - t\beta_k \geq 0$ for all k when $t \leq \min_k \alpha_k / \max(|\beta_k|, \delta)$ for any $\delta > 0$ (the minimum is taken over k with $\beta_k > 0$; if $\beta_k \leq 0$ for all k , any $t > 0$ works). Thus $\bar{\theta} + t\Delta\theta \in \mathcal{S}$. If $\bar{\theta}$ is not parallel to $\Delta\theta$, then $\bar{\theta}$ and $\bar{\theta} + t\Delta\theta$ generate distinct rays, giving $\dim(\mathcal{S}) \geq 2$. \square

Proof of Theorem 2 By Proposition 4, the stated conditions guarantee that \mathcal{S} contains at least two non-collinear vectors $v^{(1)}, v^{(2)} \in \mathcal{S}$ with $v^{(2)} \neq \alpha v^{(1)}$ for any $\alpha > 0$.

For normalization $\Theta = \{\theta : \|\theta\|_2 = 1\}$, define $\theta^{(i)} = v^{(i)} / \|v^{(i)}\|_2$. Since $v^{(1)}$ and $v^{(2)}$ are non-collinear, $\theta^{(1)} \neq \theta^{(2)}$. Both are elements of $\mathcal{S} \cap \Theta$.

By definition of \mathcal{S} , for each $k = 1, \dots, K$: $A(z^k)\theta^{(i)} \in -N_{\Omega}(z^k)$ for $i = 1, 2$. This is precisely the KKT stationarity condition $\nabla_x f(z^k, \theta^{(i)}) \in -N_{\Omega}(z^k)$ for z^k to be optimal for $\min\{f(x, \theta^{(i)}) : x \in \Omega\}$. Combined with primal feasibility $z^k \in \Omega$ and the existence of corresponding multipliers (guaranteed by the cone membership), both $\theta^{(1)}$ and $\theta^{(2)}$ rationalize all observations as optimal, hence both are feasible for \mathcal{ICCO} .

For $\mathcal{R-ICCO}$, the relaxed condition $\text{dist}(A(z^k)\theta, -N_{\Omega}(z^k)) \leq \epsilon$ is satisfied with zero distance for any $\theta \in \mathcal{S}$. Thus $\mathcal{S} \cap \Theta \subseteq \text{Feasible}(\mathcal{R-ICCO})$, and non-identifiability persists. \square

Proof of Theorem 3 Let $\theta, \theta' \in \Theta$ both be feasible for \mathcal{ICCO} with imputed optima $\{z^k\}_{k=1}^K$. By Assumption 4, the forward problem has a unique optimizer for each parameter, so the imputed

optima are determined by θ (and θ'). Since both parameters rationalize the same observations, the KKT conditions hold at each z^k :

$$A(z^k)\theta + \alpha_k n^k = 0, \quad \alpha_k \geq 0, \quad (\text{EC.1})$$

$$A(z^k)\theta' + \alpha'_k n^k = 0, \quad \alpha'_k \geq 0, \quad (\text{EC.2})$$

where we have used Assumption 5 to write $-A(z^k)\theta \in N_\Omega(z^k) = \text{cone}\{n^k\}$ as $A(z^k)\theta = -\alpha_k n^k$. Define $\Delta\theta := \theta - \theta'$ and $\Delta\alpha_k := \alpha_k - \alpha'_k$. Subtracting (EC.2) from (EC.1): $A(z^k)\Delta\theta + \Delta\alpha_k n^k = 0$ for $k = 1, \dots, K$. Apply the projection $P_k = I - n^k(n^k)^\top$ to both sides. Since $P_k n^k = 0$ (using $\|n^k\|_2 = 1$): $P_k A(z^k)\Delta\theta = 0$ for $k = 1, \dots, K$. Left-multiply by $A(z^k)^\top$ and sum over k : $\sum_{k=1}^K A(z^k)^\top P_k A(z^k)\Delta\theta = S \Delta\theta = 0$. By Assumption 6, $S \succ 0$, so $\Delta\theta = 0$, i.e., $\theta = \theta'$. The normalization $\theta \in \Theta$ removes any residual scaling or sign ambiguity. \square

Proof of Proposition 5 Suppose S is singular, so there exists $\Delta\theta \neq 0$ with $S\Delta\theta = 0$. This implies $\Delta\theta^\top S \Delta\theta = \sum_{k=1}^K \|P_k A(z^k)\Delta\theta\|_2^2 = 0$, hence $P_k A(z^k)\Delta\theta = 0$ for all k . Since $P_k A(z^k)\Delta\theta = 0$, the vector $A(z^k)\Delta\theta$ lies in $\ker(P_k) = \text{span}\{n^k\}$, so $A(z^k)\Delta\theta = \beta_k n^k$ for some $\beta_k \in \mathbb{R}$.

Let θ be any parameter satisfying the KKT conditions at $\{z^k\}$ with multipliers $\{\alpha_k\}$: $A(z^k)\theta = -\alpha_k n^k$ with $\alpha_k \geq 0$. Define $\theta' := \theta + t\Delta\theta$ for $t > 0$. Then: $A(z^k)\theta' = -\alpha_k n^k + t\beta_k n^k = -(\alpha_k - t\beta_k)n^k$.

For t sufficiently small, $\alpha'_k := \alpha_k - t\beta_k \geq 0$ for all k (since $\alpha_k > 0$ generically, or by choosing $t \leq \min_k \alpha_k / \max(|\beta_k|, 1)$). Thus θ and $\theta + t\Delta\theta$ are distinct parameters satisfying the KKT conditions at all $\{z^k\}$, demonstrating non-identifiability prior to normalization. \square

Proof of Corollary 2 For (i): Suppose $\Delta\theta \neq 0$. For each k with $A(z^k)$ full rank, $A(z^k)\Delta\theta \neq 0$. Since $\{n^k\}$ span \mathbb{R}^n , no single nonzero vector $w \in \mathbb{R}^n$ can be parallel to all n^k simultaneously (this would require $w \in \text{span}\{n^k\}$ for each k , but $n \geq 2$ linearly independent vectors cannot all be proportional to a single w). Hence there exists k such that $A(z^k)\Delta\theta$ is not parallel to n^k , giving $P_k A(z^k)\Delta\theta \neq 0$ and $\Delta\theta^\top S \Delta\theta > 0$.

For (ii): With $P_{k_0} = I$ and $A(z^{k_0})$ full rank, $S \succeq A(z^{k_0})^\top A(z^{k_0}) \succ 0$. \square

Proof of Theorem 4 Direct counting: \mathcal{IL} has decision variables $(z, \theta, \lambda) \in \mathbb{R}^n \times \mathbb{R}^p \times \mathbb{R}^m$, totaling $n + p + m$ variables. The constraints comprise m primal feasibility conditions (8b), n stationarity equations (8c), and m complementarity conditions (8d), totaling $n + 2m$ constraints. Both quantities are independent of K . \square

Proof of Proposition 6 Expanding the squared norm: $\sum_{k=1}^K \|x^k - z\|_2^2 = \sum_{k=1}^K \|x^k\|_2^2 - 2K\bar{x}^\top z + K\|z\|_2^2 = K\|z - \bar{x}\|_2^2 + \sum_{k=1}^K \|x^k\|_2^2 - K\|\bar{x}\|_2^2$. The last two terms are constant with respect to (z, θ, λ) .

\square

Proof of Theorem 5 The stationarity condition (8c) requires $A(z^*)\theta = -\sum_{i=1}^m \lambda_i \nabla g_i(z^*)$. By complementarity (8d), $\lambda_i > 0$ only if $i \in I(z^*)$. Thus $A(z^*)\theta \in -N_\Omega(z^*)$. Conversely, any θ satisfying

this inclusion admits nonnegative multipliers λ such that (z^*, θ, λ) satisfies the KKT conditions. Under Assumption 2, KKT conditions are necessary and sufficient, completing the characterization.

□

Proof of Proposition 7 By Proposition 6, \mathcal{IL} minimizes $\|z - \bar{x}\|_2^2$ subject to z being optimal for some $\theta \in \Theta$. Under Assumption 7(iv), the feasible set for z in \mathcal{U} is the convex face F . The metric projection onto a closed convex set is well-defined and unique. □

Proof of Theorem 6 (i) By the strong law of large numbers, $\bar{x} = \frac{1}{K} \sum_{k=1}^K x^k \rightarrow \mathbb{E}[x^k] = z_0$ almost surely.

(ii) For K sufficiently large, $\bar{x} \in \mathcal{U}$ almost surely. By Assumption 7(iv), $\mathcal{Z}^* \cap \mathcal{U} = F_0 \cap \mathcal{U}$ is closed and convex. The \mathcal{IL} solution satisfies $z_{\mathcal{IL}}^* = \text{proj}_{F_0 \cap \mathcal{U}}(\bar{x})$ for large K . The metric projection onto a closed convex set is nonexpansive, so $z_{\mathcal{IL}}^* \rightarrow \text{proj}_{F_0}(z_0) = z_0$, where the last equality uses $z_0 \in F_0$.

(iii) The set-valued mapping $z \mapsto N_\Omega(z)$ is outer semicontinuous for closed convex Ω (Rockafellar and Wets 2009). Since $\Theta^*(z) = \{\theta \in \Theta : A(z)\theta \in -N_\Omega(z)\}$ and $(z, \theta) \mapsto A(z)\theta$ is continuous, the mapping $z \mapsto \Theta^*(z)$ is outer semicontinuous by composition. □

Proof of Proposition 8 Both $z_{\mathcal{IL}}^*$ and z_{out}^* are projections onto the same convex face F_0 . The projection onto a convex set is 1-Lipschitz. □

Proof of Theorem 7 The objective $\|z - \bar{x}\|_2^2$ is strictly convex in z . By Assumption 7(iv), the feasible set $\mathcal{Z}^* \cap \mathcal{U}$ coincides locally with the convex set F_0 . A strictly convex function minimized over a convex set has a unique minimizer. Consistency follows from Theorem 6. □

Proof of Proposition 9 (i)–(ii): \mathcal{IL} uniqueness (Theorem 7) requires only strict convexity of the objective and local convexity of the feasible set $\mathcal{Z}^* \cap \mathcal{U}$. Neither involves normal cone dimension or excitation matrices.

(iii): For polyhedral Ω , faces are convex. If $z_0 \in \text{relint}(F_0)$ and there exists $\theta \in \Theta$ such that $F_0 \subseteq \arg \min_{x \in \Omega} \theta^\top x$, then locally \mathcal{Z}^* coincides with F_0 , satisfying Assumption 7(iv). This condition can hold even when the normal cone at z_0 is high-dimensional and excitation fails. Conversely, classical \mathcal{IO} conditions (Assumptions 5–6) can hold even when \mathcal{Z}^* is not locally convex near z_0 . □

Proof of Corollary 3 By Theorem 6, $z_{\mathcal{IL}}^* \rightarrow z_0$. By Theorem 3, $\Theta^*(z_0) = \{\theta_0\}$ under the stated assumptions. By outer semicontinuity of $z \mapsto \Theta^*(z)$, we have $\Theta^*(z_{\mathcal{IL}}^*) \rightarrow \Theta^*(z_0) = \{\theta_0\}$. □

Proof of Proposition 10 (i) The preimage of a convex cone under a linear map is convex; intersection with the convex set Θ preserves convexity.

(ii) For polyhedral Ω , $N_\Omega(z^*) = \text{cone}\{a_i : i \in I(z^*)\}$ is polyhedral. The condition $A(z^*)\theta \in -N_\Omega(z^*)$ becomes: there exist $\mu_i \geq 0$ such that $A(z^*)\theta = -\sum_{i \in I(z^*)} \mu_i a_i$, defining a polyhedron in (θ, μ) -space; projecting onto θ yields a polyhedron.

(iii) With $N_\Omega(z^*) = \text{cone}\{n^*\}$, applying P_{n^*} to the constraint $A(z^*)\theta = -\alpha n^*$ gives $P_{n^*} A(z^*)\theta = 0$. The solution set has dimension $p - \text{rank}(P_{n^*} A(z^*))$; intersecting with $\|\theta\|_2 = 1$ reduces dimension by 1. □

Proof of Theorem 8 (a) By Assumption 10, there exists $z \in \Omega$ with exactly r active relevant constraints, strict slack on inactive ones, LICQ, and a valid (θ, λ) pair. Setting $v_i = 1$ for active relevant constraints and $v_i = 0$ otherwise satisfies all constraints of \mathcal{GIL} , including the slack requirement (13e).

(b) The objective is continuous, the feasible set is a finite union of closed sets (indexed by binary vectors satisfying (13h)), and Ω is compact. By the Weierstrass theorem, an optimum exists.

(c) By Remark 7, any feasible solution satisfies the KKT conditions. Under Assumption 2, KKT is sufficient for optimality. \square

Proof of Theorem 9 By the slack constraint (13e), $v_i^* = 0$ implies $g_i(z^*) \leq -\varepsilon < 0$ for $i \in \mathcal{R}$. Thus $g_i(z^*) = 0$ implies $v_i^* = 1$ for relevant constraints. Conversely, $v_i^* = 1$ forces $g_i(z^*) = 0$ by (13f). The stationarity and complementarity analysis then follows identically to Theorem 5. \square

Proof of Theorem 10 At iteration $\ell + 1$, constraint (15d) restricts the feasible region to solutions where all constraints active at z_ℓ remain active. Constraint (15i) further requires at least one additional relevant constraint to bind. Thus the feasible set at iteration $\ell + 1$ is contained in (and generically a proper subset of) the feasible set at iteration ℓ . Since both problems minimize the same objective, optimization over a smaller feasible set yields a weakly larger optimal value. \square

Proof of Theorem 11 By (15d), $\mathcal{A}_\ell \subseteq \mathcal{A}_{\ell+1}$: all constraints active at iteration ℓ remain active at $\ell + 1$, and (15i) ensures at least one additional constraint activates. The defining equalities of $\mathcal{F}_{\ell+1}$ include all those of \mathcal{F}_ℓ plus additional ones, yielding containment. \square

Proof of Theorem 12 In the linear case with $\phi_j(x) = x_j$, the gradient matrix $A(z) = I_n$ is the identity (independent of z), since $\nabla \phi_j(z) = e_j$ for all z . At each iteration, \mathcal{MGL} enforces stationarity $\theta = A^\top \lambda = \sum_i \lambda_i a_i$. By Theorem 11, $\mathcal{A}_\ell \subseteq \mathcal{A}_{\ell'}$ for $\ell \leq \ell'$. Any $\theta \in \text{cone}\{a_i : i \in \mathcal{A}_\ell\}$ can be written as a nonnegative combination of normals from $\mathcal{A}_\ell \subseteq \mathcal{A}_{\ell'}$. Since all constraints in $\mathcal{A}_{\ell'}$ are active at $z_{\ell'}$, stationarity holds with appropriate multipliers, making $z_{\ell'}$ optimal for θ . \square

Proof of Theorem 13 By induction. At $\ell = 0$, $z_0^K \rightarrow z_0^0 = z_0$ by \mathcal{IL} consistency (Theorem 6). At iteration $\ell + 1$, the feasible set is determined by $\mathcal{A}(z_\ell^K)$, which converges to $\mathcal{A}(z_0^\ell)$ under non-degeneracy as $z_\ell^K \rightarrow z_\ell^0$. The optimization is continuous in the defining constraints, so $z_{\ell+1}^K \rightarrow z_{\ell+1}^0$. \square

Proof of Theorem 14 Under the feasibility assumption, z^{FO} lies in the feasible set of \mathcal{GIL} (it has exactly r active relevant constraints with all others strictly slack, and satisfies KKT by construction). \mathcal{GIL} minimizes aggregate distance over this feasible set, so z_{GIL}^* achieves weakly smaller objective value. \square

EC.2. Decision-Support Tools

To translate the \mathcal{IL} framework into operational tools, we developed two interactive web-based applications.

Personalized Nutrition Recommender (optimal-lab.com/nutrition-recommender). This tool allows users (patients, dietitians) to input a daily food intake, select a dietary regimen (DASH, low-carb, etc.), and specify preferred constraints \mathcal{P} . The tool applies the *MGIL* model iteratively, presenting a sequence of recommended modifications (Figures EC.1–EC.2) that visualize the observation-constraint tradeoff path. Each step shows the concrete food group changes needed to satisfy an additional nutritional target, facilitating shared decision-making between patient and clinician.

Optimal Diet Dashboard (optimal-lab.com/optimal-diet). This research tool enables exploration of retrospective results from the NHANES dataset. Users select demographic subgroups, apply *GIL* or *MGIL* with varying parameters (r , \mathcal{P}), and compare recommended versus observed diets. Figure EC.3 illustrates the interface, which supports population-level analysis of adherence patterns and intervention strategy evaluation.

These tools operationalize the theoretical framework by providing flexible, interpretable, and personalized recommendations that bridge the gap between evidence-based guidelines and individual dietary behavior.

EC.3. Diet Recommendation Problem Additional Data and Results

This section includes additional information on the input data for the diet recommendation problem and figures indicating *GIL* solutions for all food types and nutrients. The intake data include more than 5,000 different food types. Given the large number of food types, we bundled them into 38

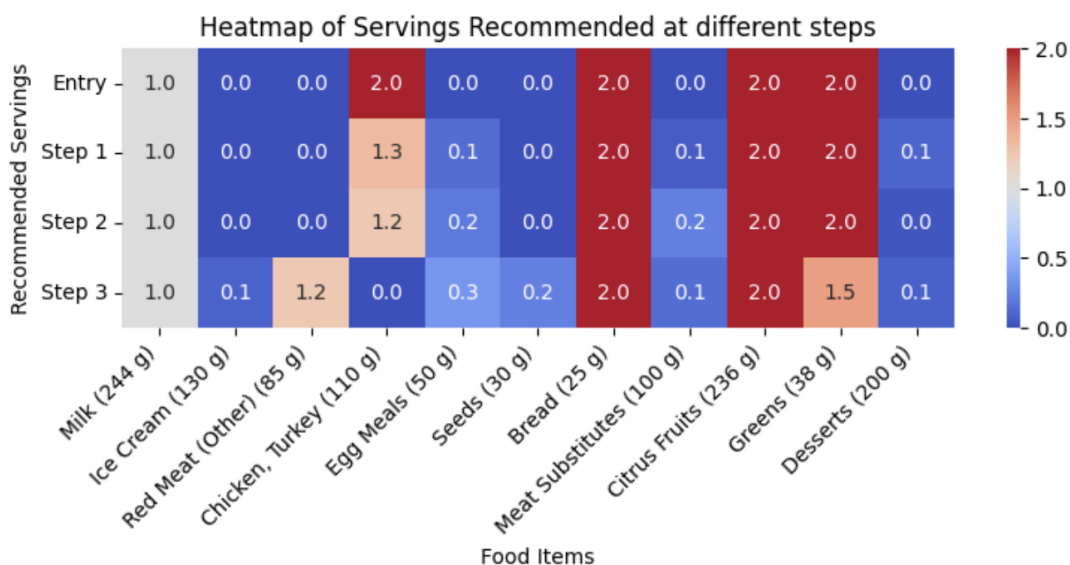


Figure EC.1 Interactive diet recommendation tool: recommended food group modifications at each *MGIL* iteration. Row 1 shows the user’s input; subsequent rows represent sequential “nudges” that bind additional nutritional constraints.

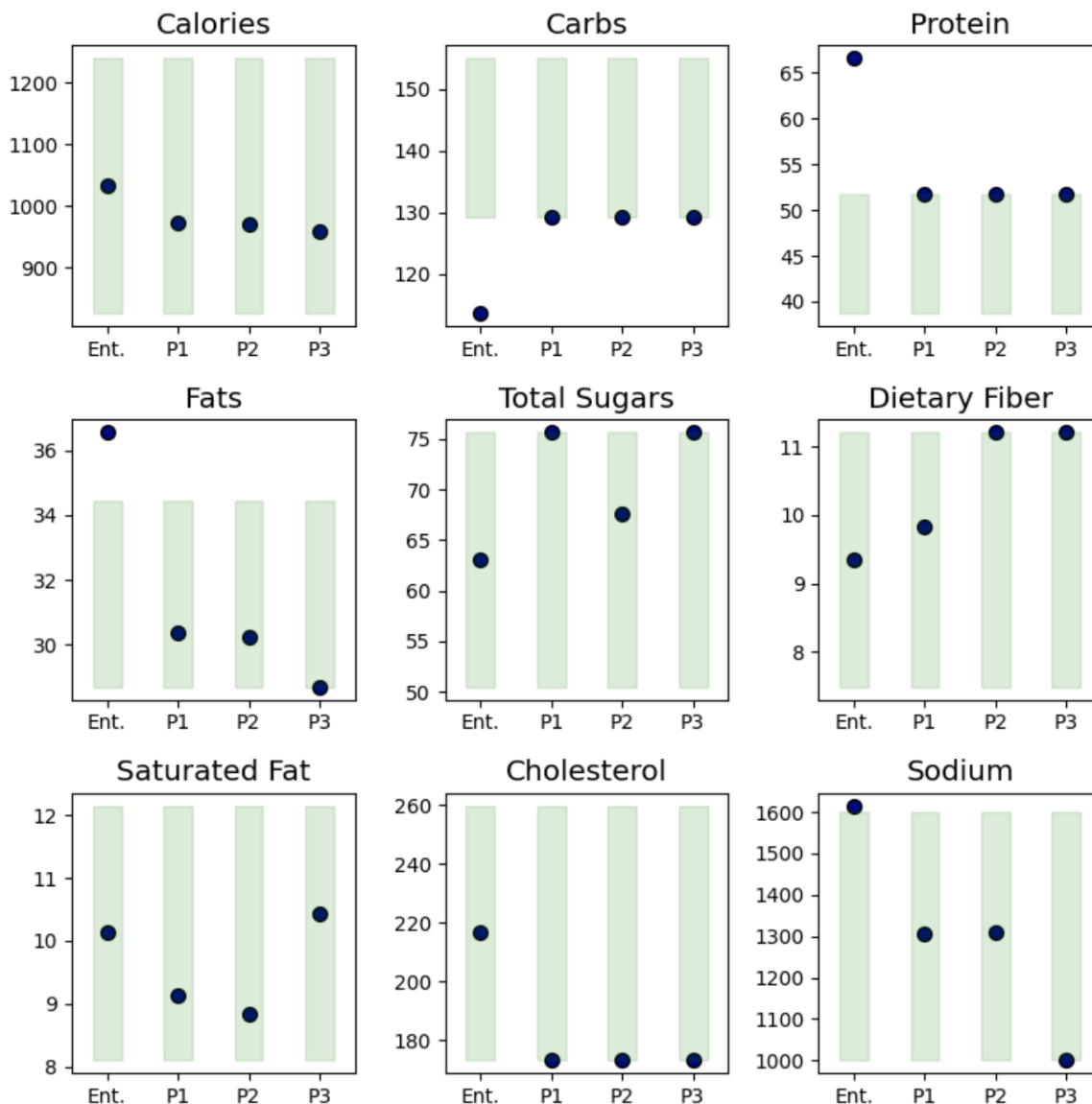


Figure EC.2 Nutrient profiles at each *MGLC* step. Step 1 maximizes protein (per user preference), Step 2 maximizes dietary fiber, and Step 3 reduces sodium to the DASH target, illustrating the structured tradeoff navigation enabled by preferred constraints \mathcal{P} .

broad food groups for ease of interpretation and to make the learned diets more tractable. This categorization is done based on the food codes from USDA. Table EC.1 shows the grouping developed for the dataset and the average serving size of each food item in grams. Table EC.2 illustrates the recommendations of the DASH diet in terms of the number of servings of each food group for different diets with distinct calorie targets. Since the DASH diet recommendations are in servings, Table EC.2 provides additional details about a typical sample of each food group along with the corresponding amount in one serving size. We utilize the food samples from Table EC.2, the nutritional data

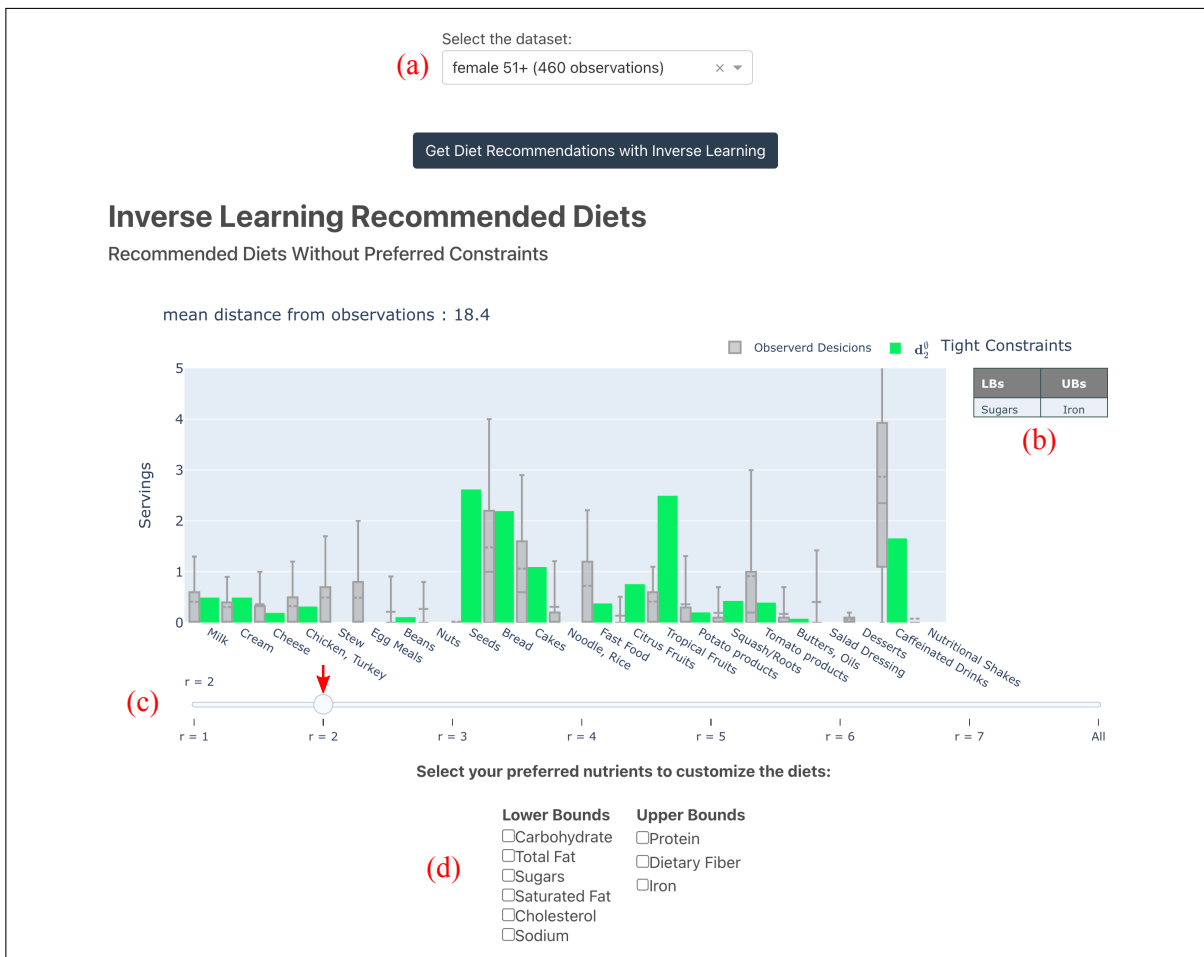


Figure EC.3 Optimal Diet Dashboard interface. (a) Dataset and subgroup selection, (b) display of binding relevant constraints, (c) slider to explore different constraint binding levels r , and (d) panel for specifying preferred constraints \mathcal{P} . The dashboard enables researchers and practitioners to analyze population adherence patterns and evaluate dietary intervention strategies within the *GIL* framework.

from USDA, and the recommended amounts from the DASH eating plan to calculate the required bounds on nutrients. These bounds can serve as the right-hand side vector for constraints in linear optimization settings. Figures EC.4 and EC.5 showcase results of applying GIL to all the data from the same population groups, showing the results of implementing inverse learning models for all food types and all nutrients. We also note that in this figure of nutrients, the lower bound of sugar is binding for the $r = 1$ of GIL and in increasing values of r , it becomes non-binding. This is due to the fact that not only the binding constraints chosen by the binary variables are forced to remain binding and any other constraint that becomes binding in addition to the ones chosen by the binary variables might become non-binding in subsequent runs with higher r values. With the increasing applications and importance of optimization and learning models, the ease of access to reliable,

accurate, and interpretable datasets has become paramount. We hope that the presence of such a dataset can help the researchers in different data-driven approaches to evaluate proposed methods and get meaningful insights.

Table EC.1 Food groups and their respective serving sizes in grams

Group Name	Description	Serving Size (g)
Milk	milk, soy milk, almond milk, chocolate milk, yogurt, baby food, infant formula	244
Cream	Cream, sour cream	32
Ice Cream	all types of ice cream	130
Cheese	all types of cheese	32
Beef	ground beef, steaks (cooked, boiled, grilled or raw)	65
Pork	chops of pork, cured pork, bacon (cooked, boiled, grilled or raw)	84
Red Meat (Other)	lamb, goat, veal, venison (cooked, boiled, grilled or raw)	85
Chicken, Turkey	all types of chicken, turkey, duck (cooked, boiled, grilled or raw)	110
Sausages	beef or red meat by-products, bologna, sausages, salami, ham (cooked, boiled, grilled or raw)	100
Fish	all types of fish,	85
Stew	stew meals containing meat (or substitutes), rice, vegetables	140
Frozen Meals	frozen meal (containing meat and vegetables)	312
Egg Meals	egg meals, egg omelets and substitutes	50
Beans	all types of beans (cooked, boiled, baked, raw)	130
Nuts	all types of nuts	28.35
Seeds	all types of seeds	30
Bread	all types of bread	25
Cakes, Biscuits, Pancakes	cakes, cookies, pies, pancakes, waffles	56
Noodle, Rice	macaroni, noodle, pasta, rice	176
Cereal	all types of cereals	55
Fast Foods	burrito, taco, enchilada, pizza, lasagna	198
Meat Substitutes	meat substitute that are cereal- or vegetable protein-based	100
Citrus Fruits	grapefruits, lemons, oranges	236
Dried Fruits	all types of dried fruit	28.3
Tropical Fruits	apples, apricots, avocados, bananas, cantaloupes, cherries, figs, grapes, mangoes, pears, pineapples	182
Fruit Juice	All types of fruit juice	249
Potato products	potatoes (fried, cooked)	117
Greens	beet greens, collards, cress, romaine, greens, spinach	38
Squash/Roots	carrots, pumpkins, squash, sweet potatoes	72
Tomato products	tomato, salsa containing tomatoes, tomato byproducts	123
Vegetables	raw vegetables	120
Puerto Rican Food	Puerto Rican style food	250
Smoothies	fruit and vegetable smoothies	233
Butter, Oils	butters, oils	14.2
Salad Dressing	all types of salad dressing	14
Desserts	sugars, desserts, toppings	200
Caffeinated Drinks	coffees, soda drinks, iced teas	240
Nutritional Shakes	Nutritional shakes, Energy Drinks, Protein Powders	166

Table EC.2 Food categories and their recommended number of servings for different targets based on the DASH diet ([DASH 2018](#))

Food Category	Diet Target						
	1,200 Calories	1,400 Calories	1,600 Calories	1,800 Calories	2,000 Calories	2,600 Calories	3,100 Calories
Grains	4–5	5–6	6	6	6–8	10–11	12–13
Vegetables	3–4	3–4	3–4	4–5	4–5	5–6	6
Fruits	3–4	4	4	4–5	4–5	5–6	6
Fat-free or low-fat dairy products	2–3	2–3	2–3	2–3	2–3	3	3–4
Lean meats, poultry, and fish	≤ 3	≤3–4	≤3–4	≤ 6	≤6	≤6	6–9
Nuts, seeds, and legumes	3/week	3/week	3–4/week	4/week	4–5/week	1	1
Fats and oils	1	1	2	2–3	2–3	3	4
Sweets and added sugars	≤ 3/week	≤3/week	≤3/week	≤5/week	≤5/week	≤2	≤2
Maximum sodium limit(mg/day)	2,300	2,300	2,300	2,300	2,300	2,300	2,300

Table EC.3 Food categories and their respective serving sizes in grams

Food Category	Serving Size (Example)
Grains	1 slice of whole-grain bread
Vegetables	1 cup (about 30 grams) of raw, leafy green vegetables like spinach or kale
Fruits	1 medium apple
Fat-free or low-fat dairy products	1 cup (240 ml) of low-fat milk
Lean meats, poultry, and fish	1 ounce (28 grams) of cooked meat, chicken or fish
Nuts, seeds, and legumes	1/3 cup (50 grams) of nuts
Fats and oils	1 teaspoon (5 ml) of vegetable oil
Sweets and added sugars	1 cup (240 ml) of lemonade

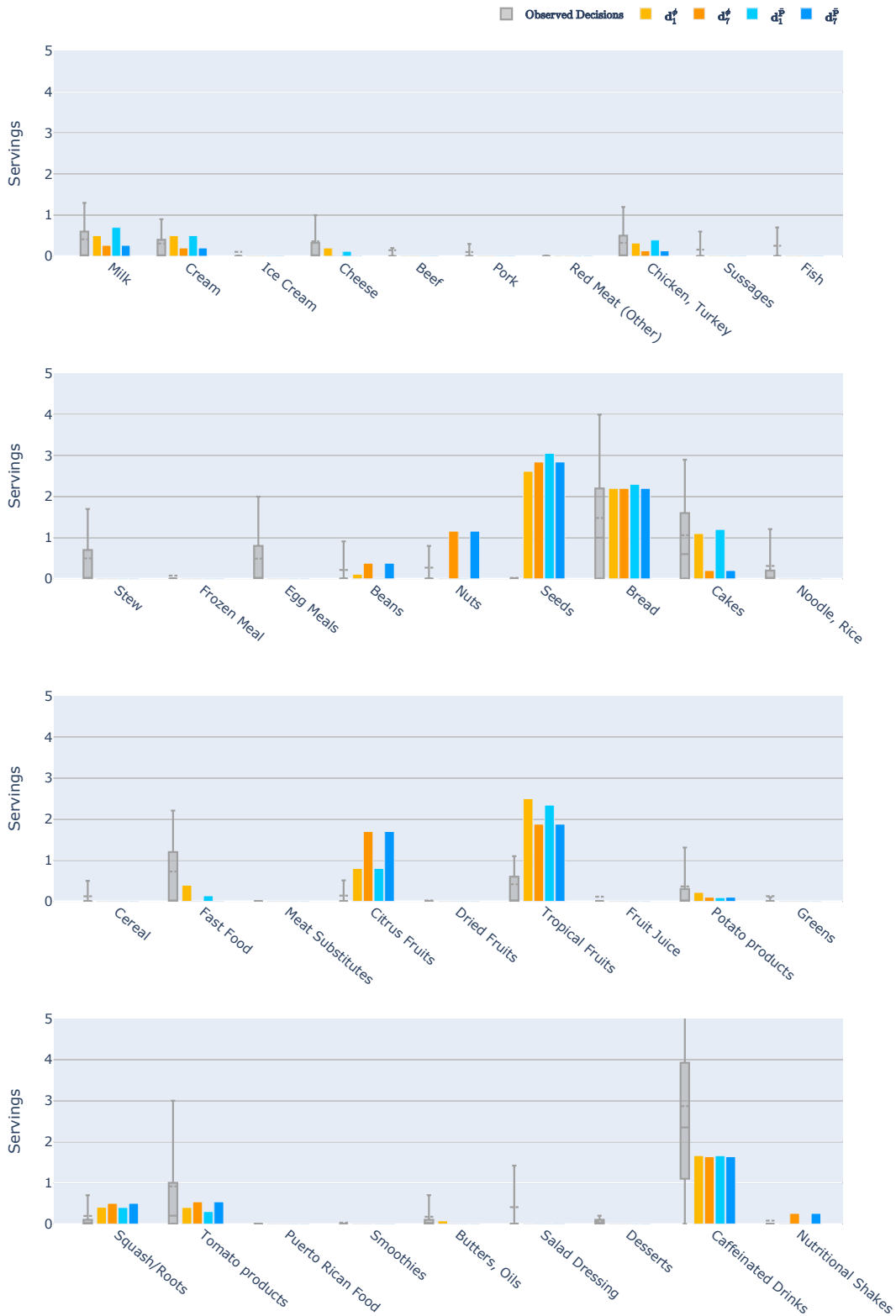


Figure EC.4 Comparison of recommended diets by GIL with different values for r and a set of 460 observations for all food types.

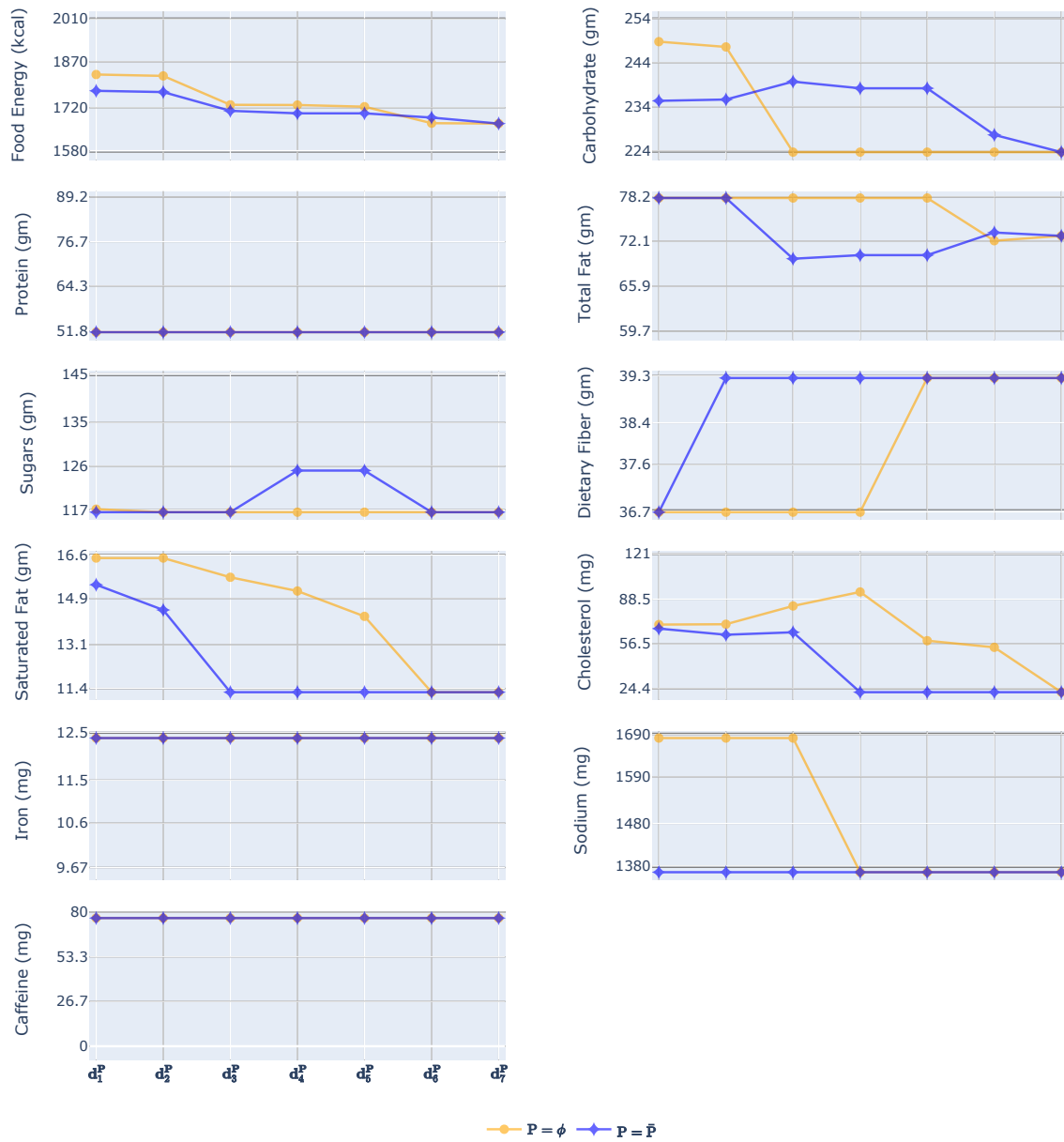


Figure EC.5 Comparison of nutrients of recommended diets by IL^0 and GIL for different values of r for all nutrients in the model. (Triv.: trivial constraint, Rel.: relevant constraint, Pref.: preferred constraint)